RM A54A05

RESEARCH MEMORANDUM

AN EVALUATION OF TWO COOLING-AIR EJECTORS IN FLIGHT AT TRANSONIC SPEEDS

By L. Stewart Rolls and C. Dewey Havill

Ames Aeronautical Laboratory
Moffett Field, Calif.

NATIONAL ADVISORY COMMITTEE
FOR AERONAUTICS

WASHINGTON
March 15, 1954

NATIONAL ADVISORY COMMITTEE FOR AERONAUTICS

RESEARCH MEMORANDUM

AN EVALUATION OF TWO COOLING-AIR EJECTORS IN FLIGHT AT TRANSONIC SPEEDS

By L. Stewart Rolls and C. Dewey Havill

SUMMARY

Flight tests conducted on the YF-93 airplane afforded an opportunity to evaluate two cooling-air ejectors of widely different geometry. One ejector had a diameter ratio (fuselage-exit diameter divided by tail-pipe diameter) of 1.58 and a spacing ratio (distance from tail-pipe exit to fuselage exit divided by tail-pipe diameter) of 0.73 while the other ejector had a diameter ratio of 1.33 and a spacing ratio of 0.30. The larger tail exhibited poor net thrust performance due to excessive quantity of secondary air flow. The second engine-ejector combination had superior characteristics; however, an undesirable characteristic existed in that a region of reversed flow was present in the exit. This reversed flow caused a decrease in the performance of the ejector.

Correlation of the flight data with cold-jet-model ejector data has demonstrated to what extent the model tests can be used as a design tool. When comparing the ejector with reversed flow with the model tests, it was necessary to consider the effect the reversed flow had on reducing the effective diameter ratio. Airplane drag measurements as determined for the widely different configurations indicated a good over-all precision for the method used in this investigation.

INTRODUCTION

The use of afterburners with turbojet engines for thrust augmentation requires a supply of cooling air flow around the engine tail pipe. One means used to supply cooling air is the jet-actuated ejector. Since afterburners are equipped with methods for varying their exit area, the job of designing an ejector is difficult, because when the geometry of the ejector is selected for the afterburner-on operating condition an excessive amount of cooling air may be pumped during afterburner-off operation. This disadvantage of the jet-actuated ejector as a means of supplying cooling air appears as a loss in net thrust.

To determine the influence of the ejector characteristics on the performance of the engine-ejector combination two cooling-air ejectors, of significantly different design, were flight tested on the YF-93 airplane. The effect of small additional changes to the ejector was also studied. These flight data afforded an opportunity to compare full-scale ejector data with the model ejector data of references 1 and 2. This investigation covered tests of the engine in combination with the cooling-air ejector in the flight Mach number range of about 0.70 to 0.98.

SYMBOLS AND NOMENCLATURE

The following symbols and nomenclature used in this report are defined in the accompanying schematic sketch of a cooling-air ejector. It should be noted that primary refers to the engine nozzle and secondary denotes the annulus between the engine tail pipe and the fuselage.

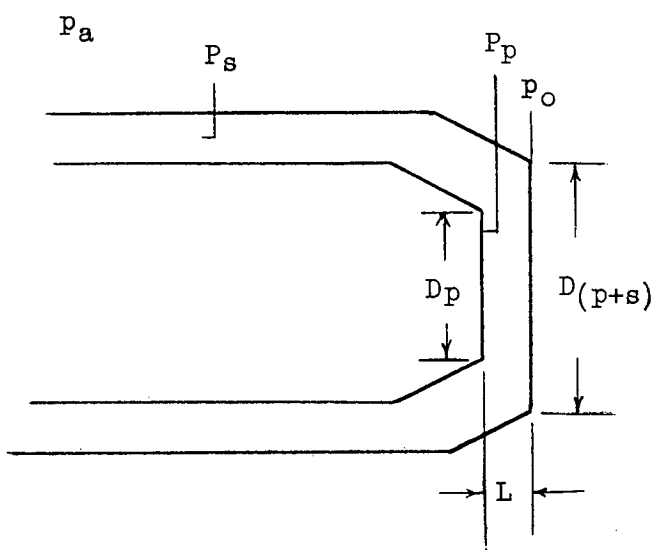

A	radial area, sq ft
C_D	chord-force coefficient
C_N	normal-force coefficient
D	diameter, ft
$\frac{D_{(p+s)}}{D_p}$	ejector diameter ratio

F_G	gross thrust, lb
F_N	net thrust, lb
L	length from tail-pipe exit to fuselage exit, ft
$\frac{L}{D_p}$	spacing ratio
M	Mach number
N	engine rotational speed, rpm
P	local total pressure, lb/ft^2
p	local static pressure, lb/ft^2
p_o	ambient exhaust pressure, lb/ft^2
p_a	atmospheric pressure, lb/ft^2
$\frac{P_p}{p_o}$	primary pressure ratio
$\frac{P_s}{p_o}$	secondary pressure ratio
T.P.T.	indicated tail-pipe temperature
t	time, sec
W	air-flow rate, slugs/sec
γ	ratio of specific heats
θ	temperature, deg Rankine
$\sqrt{\frac{\theta_s}{\theta_p}}$	air-flow temperature correction factor

Subscripts

p	primary
p+s	primary and secondary
s	secondary

DESCRIPTION OF AIRPLANE

The pertinent dimensions of the YF-93 airplane used in this investigation are listed in table I. During these tests a Model J-48-1 turbojet engine was installed in the airplane. Figure 1 is a photograph and figure 2 a two-view drawing of the test airplane. A close-up view of the two rear fuselage sections showing the changes in external lines and size is presented in figure 3. It should be noted that in figure 3(b) the primary tail pipe and eyelids are not shown. The two photographs of figure 3(b) are to the same scale and the diameter of the shroud is the same on both tails; thus, the effect of the rear fuselage modification on the exit diameter can be seen. Figure 4 is a schematic cross-sectional drawing of the rear fuselage showing the location of the tail pipe, eyelid doors, and shroud with reference to the fuselage.

Tail A has a diameter ratio of 1.58, a spacing ratio of 0.73, and has three areas of air flow. In addition to the main jet flow in the primary system it has two passages of cooling air flow, one area between the tail pipe and the shroud and a second area between the shroud and the inside of the fuselage skin. It should be pointed out that in this rear fuselage the forward end of the shroud is open. Thus, the shroud acts as a radiation shield mounted in the secondary flow region and does not establish a region of tertiary flow. The cooling air is supplied from two submerged inlets at fuselage station 313.5 and from two submerged inlets at fuselage station 404.5.

Tail B was derived from Tail A by decreasing the diameter ratio to 1.33 and the spacing ratio to 0.30. This was done by changing the fuselage lines so as to eliminate the cooling air passage between the shroud and the fuselage. Hence, on Tail B only one passage for cooling air flow is present, between the shroud and the tail pipe, and this passage is supplied air from two submerged inlets at fuselage station 313.5.

INSTRUMENTATION AND TESTS

Standard NACA recording instruments and a recording oscillograph synchronized at 1/10-second intervals by a single timing circuit were used to record the test data. True Mach number was calculated from a calibrated measurement of free-stream total and static pressures obtained with a 12.5-foot nose boom.

The instrumentation for this investigation included the fixed air-cooled total-pressure probe in the tail pipe and the swinging total-static-pressure and temperature probe which are shown on figure 5. A description of the probes and the methods used to reduce these data are presented in reference 3. The thermocouple details and the method for reducing its

output as presented in reference 3 were modified during the investigation presented in this report. A cross-sectional drawing of the redesigned thermocouple, showing its details, is presented in figure 6. The major changes made in this thermocouple over the one shown in reference 3 are: (1) A thermocouple was mounted in the shield of the main thermocouple, (2) the lead-in wires from the main thermocouple were made 50 diameters long to minimize conduction losses, and (3) barriers were placed in front of the thermocouple which allowed jet gases to enter but did not allow direct radiation from the tail to the thermocouple.

The reason for using the swinging total-static-pressure and temperature probe in place of the more conventional fixed probe was the very high jet temperature (about 3500° R) accompanying afterburner operation. The use of the swinging probe made the measurement of jet temperature difficult. To determine the actual variation of temperature across the tail pipe from the temperature indicated from the thermocouple output, a series of calibration runs were made. The true temperature profile was established by taking records with the probe at various fixed positions in the jet. The runs with the swinging probe at various fixed positions in the jet were made in flight at $M = 0.6$ and 0.8 and the records were taken after the thermocouple reached equilibrium with the exhaust gas temperature. Using these steady-state temperature profiles and the transient profiles obtained by swinging the probe through the jet, the following experimentally determined equation for relating the thermocouple output and the steady-state temperature was derived:

$$\theta_{gas} = \theta_{thermocouple} + \frac{k \frac{d\theta_{shield}}{dt}}{\text{jet static pressure}}$$

If the Mach number of the jet was less than 1.0, free-stream static pressure was used in the equation; however, if the jet Mach number was greater than 1.0, the pressure behind a normal shock was used in the equation for jet static pressure. The value of k determined in this investigation was 2080 for θ in degrees Rankine and static pressure in pounds per square foot.

To measure secondary pressure ratios in the ejector, three total-pressure tubes spaced 120° apart were mounted in the fuselage between the secondary air inlets and the exit, and three static orifices were located around the inner periphery of the exit. These pressures were measured with pressure cells with a range from 0 to 15 pounds per square inch.

The data presented in this report were obtained during runs at various fixed tail-pipe temperatures at constant Mach number. The range of test altitude during the tests was 22,000 to 27,000 feet.

The precision of the measurements estimated from the least count of the instruments and from the average scatter and repeatability of the data are:

Mach number	±0.01
Pressure altitude	±150 feet
Drag coefficient	±0.0010
Gross thrust ratio	±0.01
Net thrust ratio	±0.03
Air-flow ratio	±0.03

RESULTS AND DISCUSSION

The discussion of the flight data will be separated into three phases: the ejector characteristics, comparison between flight tests and model tests, and airplane drag measurement.

Ejector Characteristics

Tail A, afterburner off.- A typical set of data obtained on Tail A with the afterburner off is presented in figure 7. Here are shown the variations of the total pressure, static pressure, and stagnation temperature with radial position. While these data were obtained during a complete traverse of the jet, in figure 7 the curves have been folded about the jet center line. The difference between the left and right sides of the jet indicates the lag effect and amount of uncertainty in the data, which is seen to be small. It was assumed that for the circular exit of this tail pipe there was axial symmetery of pressures and temperature existing in the jet; thus, the conditions measured across one arc of the survey could be applied to the exit area.

Using the profile data as shown in figure 7 and the equations of reference 3, the gross thrust per unit area and the exhaust air flow per unit area were computed. To obtain the gross thrust and the total air flow of the ejector system, the thrust and air flow per unit area were plotted as a function of the radial area, as shown in figure 8, and integrated. Net thrusts were obtained from the gross thrust by subtracting the ram drag of the measured primary and secondary air flows. The method for determining ram drag in this report charged the losses in the boundary layer along the fuselage ahead of the secondary air inlets to the ejector; however, in light of the drag measurements to be discussed later this quantity is thought to be small. During this investigation, since the main interest was the performance of the primary and secondary systems, the area used for the integration was the fuselage exit area. The primary

thrust and air flow were computed for each run from the measurements from the fixed probe by the method outlined in reference 3.

The thrust and air-flow characteristics of the ejector incorporated in Tail A are presented in figure 9 as a function of flight Mach number. In this figure are presented the gross thrust ratios, net thrust ratios, and air flow ratios for two values of engine tail-pipe temperature. These data show that the gross thrust ratio at a Mach number of 0.70 is about 1.02 and decreases slightly with increasing Mach number. The gross thrust ratio decreases with decreasing engine tail-pipe temperature. The net thrust ratios as determined with Tail A are approximately 0.58 for maximum tail-pipe temperature and are lower for the lower tail-pipe temperatures. The reason for these low net thrust ratios can be seen in figure 9(b) where it is shown that the secondary air flow is approximately 60 percent of the primary air flow. Since the secondary air inlets would choke at an air flow of approximately 25 percent, it is necessary to assume that a large portion of this air flow must come from leakage past the plenum-chamber seal or possibly through the fuselage. It is the decrease in momentum of this cooling air from the free-stream conditions which causes Tail A to have such poor net thrust characteristics.

Ejector performance data for an indicated tail-pipe temperature of 600° C (fig. 9) show a reduction in net thrust ratio below that for 710° C. This reduction in net thrust ratio is caused by the decrease in tail-pipe temperature reducing the primary thrust while the secondary air flow ratio remains approximately the same. Therefore, the ram drag of the secondary air becomes a larger percentage of the gross thrust and the net thrust ratio is decreased.

Tail A, afterburner on.- A typical set of pressure and temperature profiles for Tail A with the afterburner operating is presented in figure 10. Typical profiles of thrust and air flow per unit area calculated from the profiles of figure 10 are presented in figure 11. The calculated performance characteristics of the ejector in Tail A with the afterburner operating are presented in figure 12. A comparison of the characteristics presented in figures 9 and 12 shows that the ejector has much better performance with the afterburner on than it has with the afterburner off. This increase in performance corresponds to an increase in net thrust ratio of about 28 percent, at a Mach number of 0.74.

Tail A modifications.- The data for Tail A with the afterburner off indicated that certain changes could be made to the rear-fuselage-ejector combination which might improve its over-all performance. As these data indicated a large amount of secondary air flow, a method to reduce this air flow was sought. One method tried was to seal off two of the four secondary inlets. The ejector performance as determined with the two inlets sealed is presented in figure 13. As was expected, the sealing of the secondary air inlets reduced the secondary air flow as shown in

figure 13(b). This reduction in secondary air flow caused a slight decrease in the gross thrust ratio; however, the over-all effect was an increase in the net thrust ratio for the ejector.

Tail B, afterburner off.- Typical profiles similar to the type presented for Tail A in figure 7 are presented in figure 14 for Tail B. The corresponding thrust and air-flow profiles are presented in figure 15. As can be seen in figure 14, there is a region in the secondary system where the pressure measured by the total-pressure probe is less than the pressure measured by the static orifices. To perform the thrust and air-flow calculations from these data it was arbitrarily assumed that the direction of the air flow was reversed. There was not sufficient instrumentation installed in the airplane to determine the exact type of reversed air flow.

Ejector performance curves were computed for Tail B and are presented in figure 16. The gross thrust ratio determined for Tail B with a tail-pipe temperature of 710° C varies from 1.08 at a Mach number of 0.7 to 0.93 at a Mach number of 0.94. The variation of net thrust ratio is from 0.98 to 0.89. The secondary-air-flow ratio was constant over the range of test Mach numbers. This value of secondary air flow was equal to 6 percent of the primary air flow. Tests performed by the manufacturer on Tail B indicated that the cooling on this tail was marginal. A slight reduction was noted in all ratios when the tail-pipe temperature was reduced to 675° C.

Tail B, afterburner on.- A typical set of data obtained on Tail B with the afterburner on is presented in figures 17 and 18. The ejector characteristics for Tail B, afterburner on, as shown in figure 19 indicate that the ejector was operating efficiently. The net thrust ratio varies from 1.15 to 1.03 over the Mach number range tested. This shows that the secondary air flow is augmenting the primary thrust in this case and is not causing the large thrust losses as noted on the other tail. Cooling was adequate on Tail B with the afterburner on.

Tail B modifications.- The pressure profiles for Tail B with the afterburner off (fig. 14) indicated an area of reversed flow. In an effort to increase the total pressure in the secondary system, scoops were mounted on the submerged, secondary air inlets. The ejector characteristics as measured with this modification are presented in figure 20. Here it is indicated that the addition of the scoops increased the gross thrust ratio and air-flow ratio; however, the net effect was negligible in regard to the net thrust. The scoops were unable to increase the measured total pressure in the secondary system above the measured static pressure; thus, the addition of the scoops did not eliminate the reversed flow. Possible modifications to the rear-fuselage-ejector combination which might improve the performance of this ejector would be to increase the spacing ratio. (The results of refs. 1 and 2 indicate a longer spacing ratio would pump

more air and thus overcome the flow reversal.) or to install additional secondary air inlets near the rear of the fuselage to increase the total pressure in the secondary air, thus overcoming the flow reversal. The inability to perform further flight tests on this airframe ruled out the possibility of testing either of these modifications during this investigation.

Comparison of Flight and Model Test

The data obtained in the present investigation have been compared with the results of references 1 and 2 for an ejector operated on a test stand. The diameter ratio for Tail A was larger than those presented in the reference report so it was necessary to extrapolate these data as shown in figure 21 to the diameter ratio of Tail A. The range of secondary pressure ratios as determined during the flight tests of the ejector is indicated on the curves for two of the conditions tested. The temperature profile shown in figure 7 shows a primary temperature of about 1650° R and a secondary temperature of about 580° R. These temperatures result in a correction factor, $\sqrt{\theta_s/\theta_p}$, of 0.59. The ejector-stand data from references 1 and 2 are for a primary pressure ratio of 2.0 which is equivalent to 0.70 Mach number data obtained during flight tests. The following table shows the comparison between the flight data (figs. 9 and 13) and the model data obtained from references 1 and 2 and plotted in figure 21.

Tail A	Basic configuration		Two inlets sealed	
	Flight	Model	Flight	Model
Gross thrust ratio	1.02	1.00 to 1.01	1.03	1.00 to 1.01
Air flow ratio	.64	.66 to .68	.61	.59 to .61

As indicated in this table, the comparison between the model tests run on an ejector test stand and the data obtained during the flight tests on Tail A is good.

The fact that Tail B exhibited a region of reversed flow in the ejector made correlation with model data difficult. Ejector-model data for a spacing ratio approximately equal to that for Tail B are presented in figure 22.

The following table shows the comparison between the flight results and the model data for Tail B. The temperatures on Tail B as shown in

figure 14 were slightly different than those on Tail A so that in this comparison a correction factor, $\sqrt{\theta_s/\theta_p}$, of 0.55 was used.

Tail B	Actual diameter ratio		Effective diameter ratio	
	Flight	Model	Flight	Model
Gross thrust ratio	1.08	1.03 to 1.05	1.08	0.99 to 1.00
Air flow ratio	.06	.31 to .33	.06	.07 to .09

The data in the table show that the comparison between the flight data and model data based on the actual diameter ratio is poor. The effective diameter-ratio criteria are based on the assumption that the reversed flow in the ejector reduces the effective diameter of the ejector. The effective diameter was determined by averaging the area of indicated reversed air flow as shown in figure 15 and subtracting this reversed-flow area from the total exit area. This effective diameter was 3.05 square feet which results in an effective diameter ratio of 1.06. By using the effective diameter-ratio criteria, correlation was obtained between flight and model tests.

Airplane Drag Measurements

Since the major portion of the airplane remained unchanged during this investigation, the changes in the tail being considered minor when referred to the total airplane, it was reasoned that the total drag of the aircraft should be equal for both tail-exit configurations. Using this assumption, the over-all precision of the net thrust determination has been evaluated by calculating the airplane drag coefficient as presented in figure 23, using the net thrust of the ejector combination. The main factor which would be changed by the modification of the rear fuselage lines would be the base-pressure drag. This effect, however, has been taken into account in the calculation of the gross thrust so that the original assumption is considered adequate.

The reliability of the method used in this investigation to determine the in-flight performance characteristics of a rear-fuselage-ejector combination is indicated in figure 23. This figure shows that the airplane drag coefficient as determined for widely different secondary air flow rates (6 percent and 60 percent of the primary air flows) and widely different ejector geometry (two tails with afterburner on and off) forms a single curve. The fact that the drag measured for the various conditions tested agrees indicates that the precision of the ejector-performance determination is good.

SUMMARY OF RESULTS

Flight tests conducted on the YF-93 airplane with two different cooling air ejectors indicated the following:

1. Tail A, which had a diameter ratio of 1.58 and spacing ratio of 0.73, had poor net thrust performance with the afterburners off, due to excess cooling air flow. Ejector performance with the afterburner operating was better than with afterburner off.

2. Tail B, which had a diameter ratio 16 percent less than Tail A (which reduced the cooling air flow) had good net thrust performance with the afterburner on and off. This tail did indicate an undesirable effect, however, in the fact that during the afterburner-off operation a region of reversed flow was measured in the secondary system.

3. Comparison of the characteristics of the ejectors as determined in flight with those determined in cold jet tests on an ejector test stand indicated good agreement between the two sets of data. When comparing Tail B with the model tests, it was necessary to consider the effect the reversed flow had on reducing the effective diameter ratio.

4. A good over-all precision is indicated for the method of evaluating the ejector performance in flight. This precision is determined from the correlation of airplane drag measurements for widely different ejector configurations.

Ames Aeronautical Laboratory
National Advisory Committee for Aeronautics
Moffett Field, Calif., Jan. 5, 1954

REFERENCES

1. Greathouse, W. K., and Hollister, D. P.: Preliminary Air-Flow and Thrust Calibrations of Several Conical Cooling-Air Ejectors with a Primary to Secondary Temperature Ratio of 1.0. II - Diameter Ratios of 1.06 and 1.40. NACA RM E52F26, 1952.

2. Greathouse, W. K., and Hollister, D. P.: Preliminary Air-Flow and Thrust Calibrations of Several Conical Cooling-Air Ejectors with a Primary to Secondary Temperature Ratio of 1.0. I - Diameter Ratios of 1.21 and 1.10. NACA RM E52E21, 1952.

3. Rolls, L. Stewart, Havill, C. Dewey, and Holden, George R.: Techniques for Determining Thrust in Flight for Airplanes Equipped With Afterburners. NACA RM A52K12, 1953.

TABLE I.- DIMENSIONS OF TEST AIRPLANE

YF-93

Wing	
Total wing area (including flaps, aileron, and 65.83 sq ft covered by fuselage)	306.10 sq ft
Span	38.90 ft
Aspect ratio	4.943
Taper ratio	0.502
Mean aerodynamic chord	98.75 in.
Sweepback angle	
Leading edge	37° 45'
25-percent element	35° 15'
Fuselage	
Length	42.75 ft
Depth, maximum	76.6 in.
Width, maximum	85.0 in.
Fineness ratio	6.125

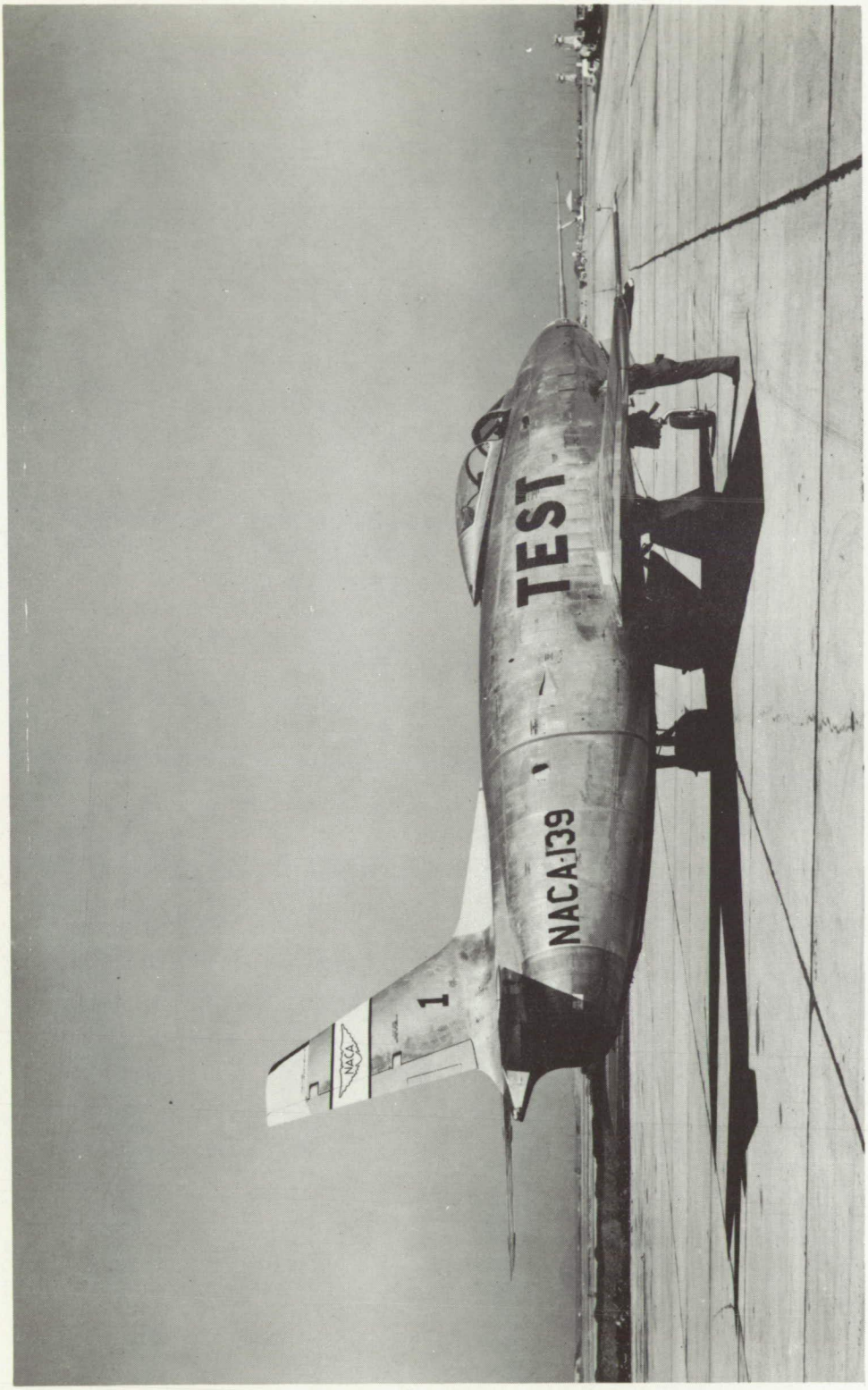

Figure 1.- Photograph of test airplane equipped with Tail B.

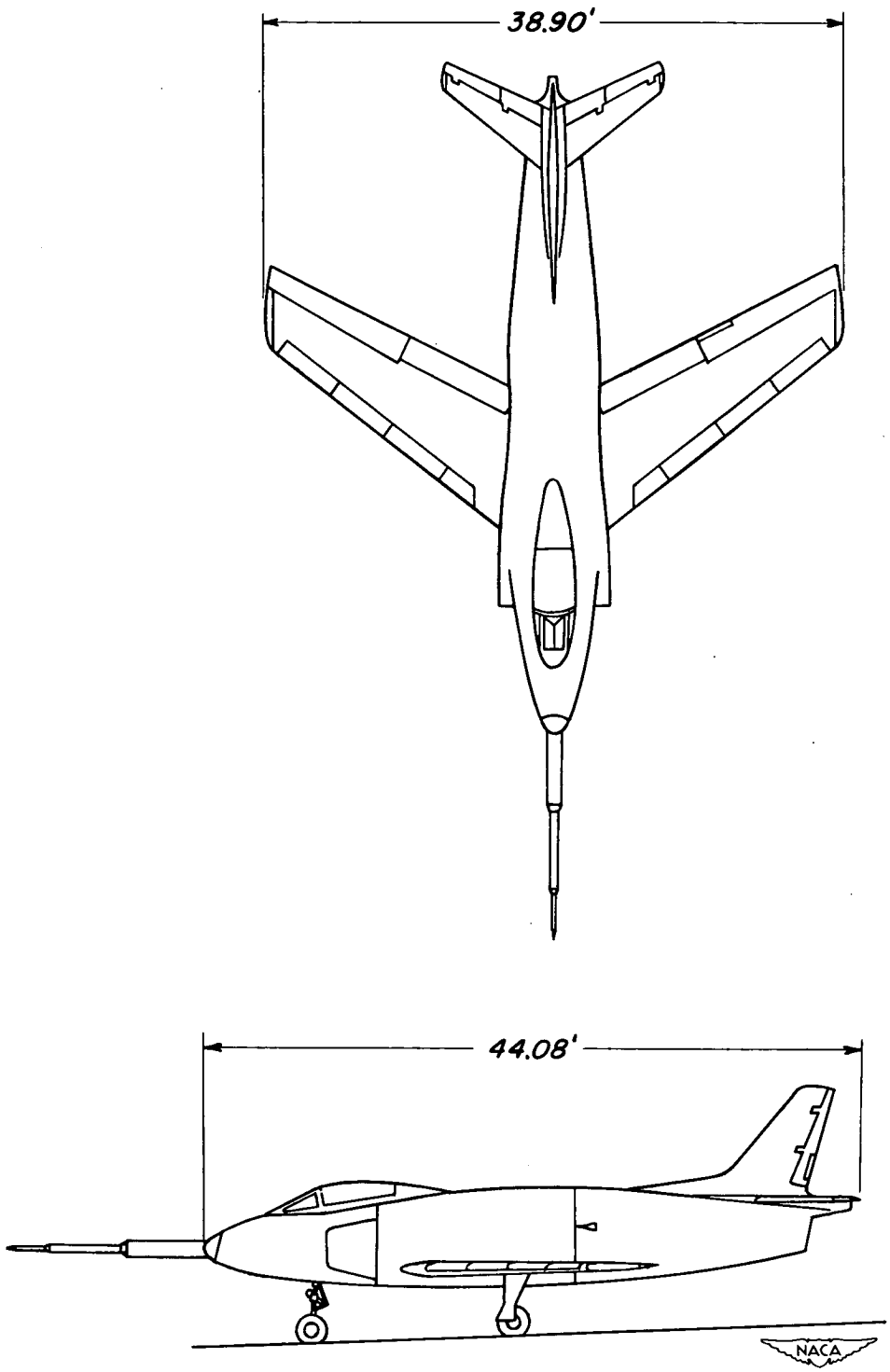

Figure 2.- Two view drawing of the test airplane with Tail B.

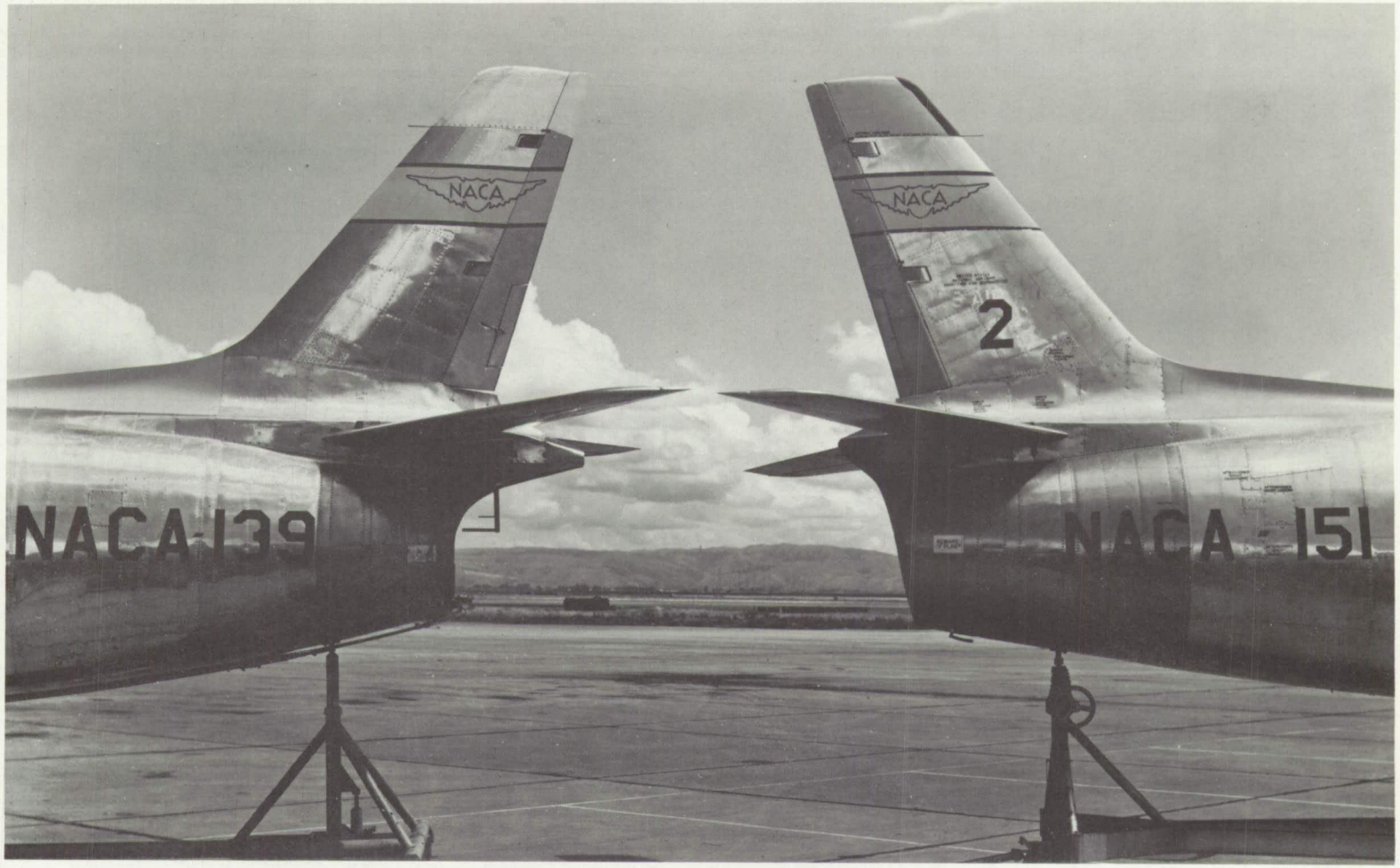

A-18243

Tail B Tail A

(a) Side view.

Figure 3.- Close-up photographs of the two rear fuselage sections.

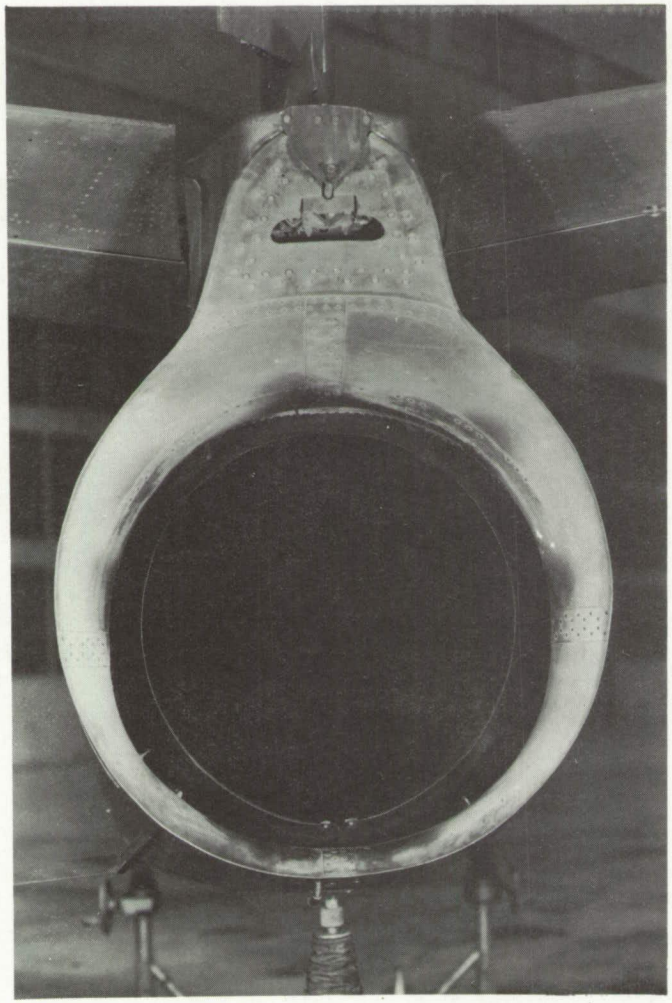

A-18308

Tail A

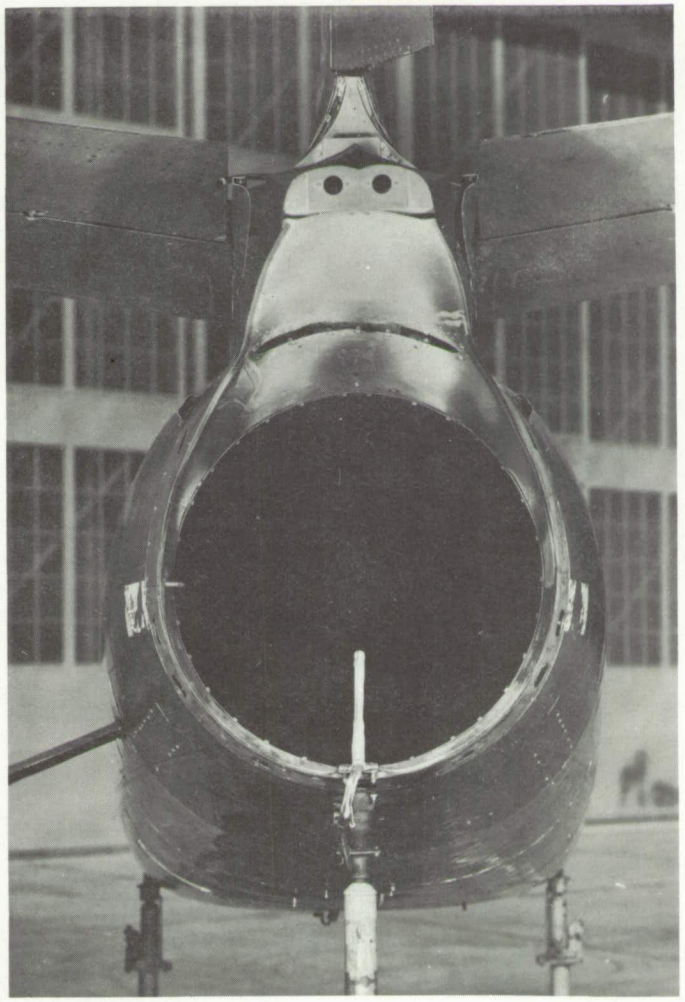

A-18309

Tail B

(b) End view.

Figure 3.- Concluded.

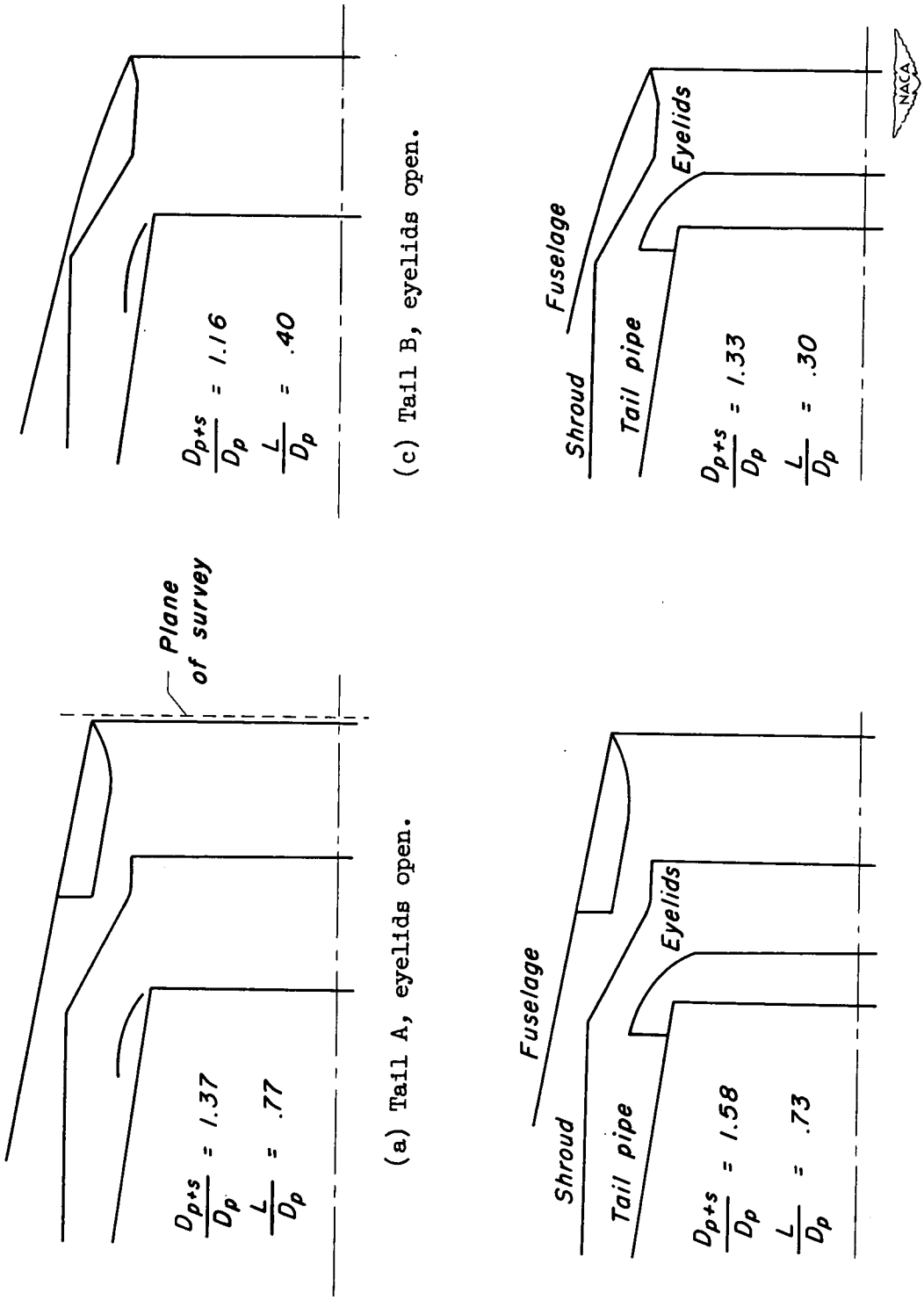

(a) Tail A, eyelids open.

(c) Tail B, eyelids open.

(b) Tail A, eyelids closed.

(d) Tail B, eyelids closed.

Figure 4.- Cross-section drawing of the two cooling air ejectors.

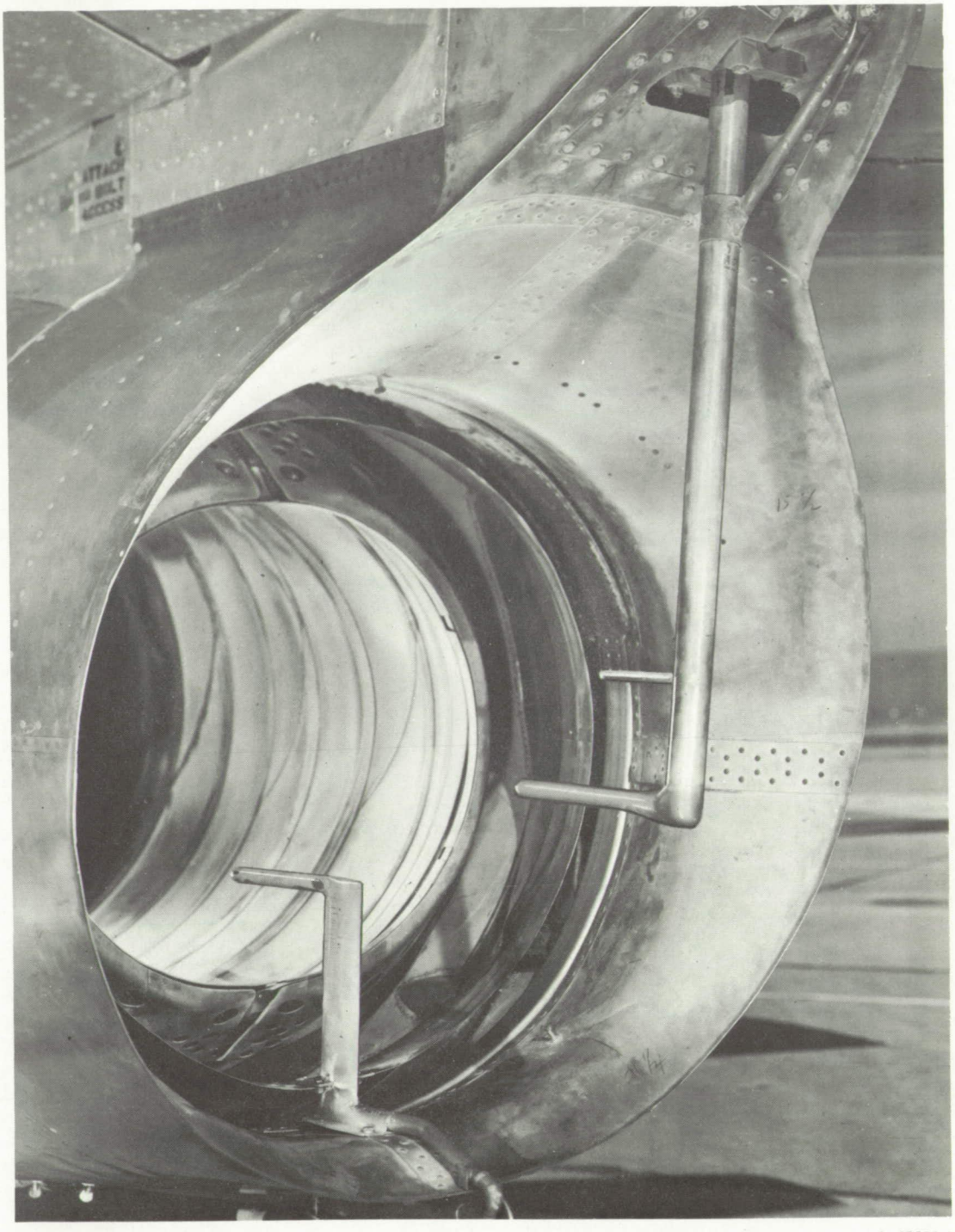

A-17823.1

Figure 5.- Photograph of instrumentation.

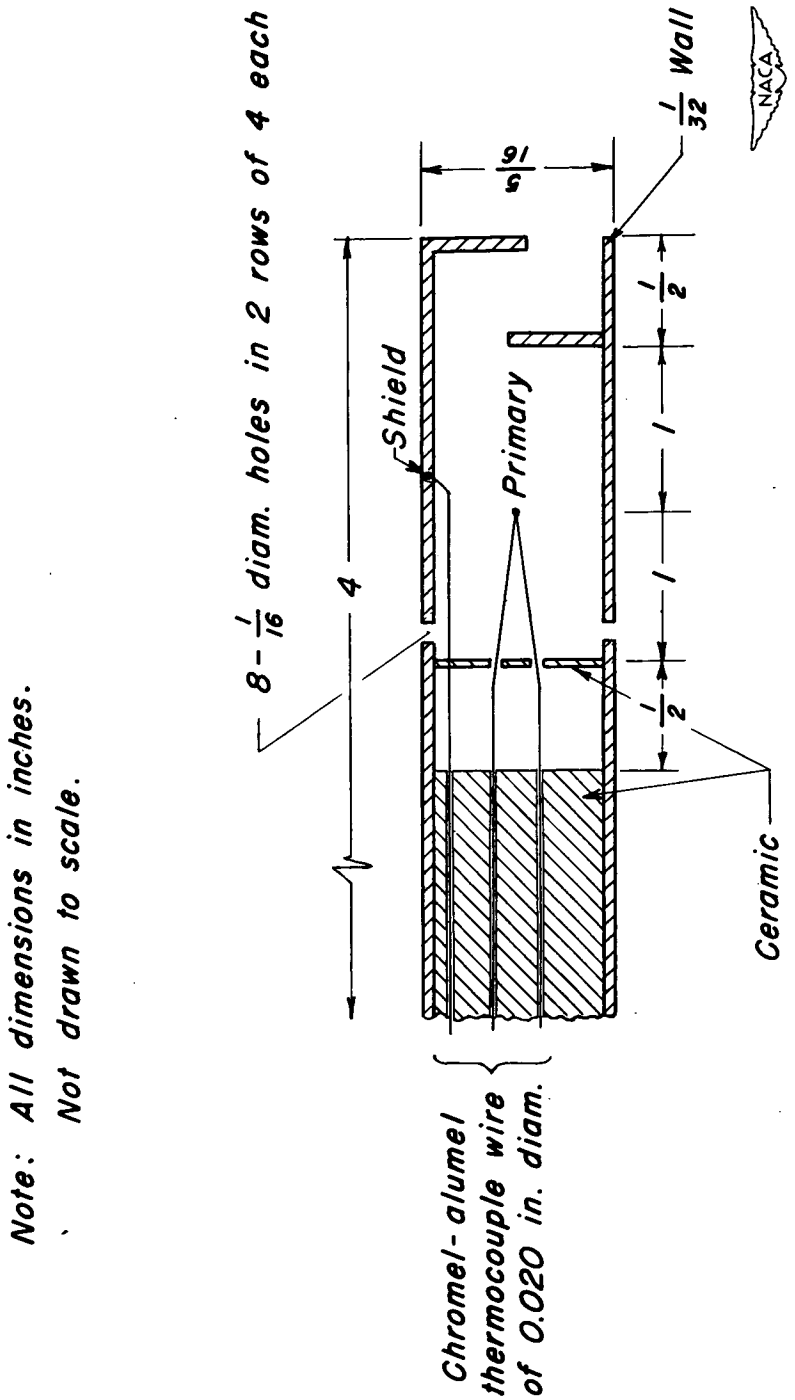

Figure 6.- Details of the stagnation thermocouple.

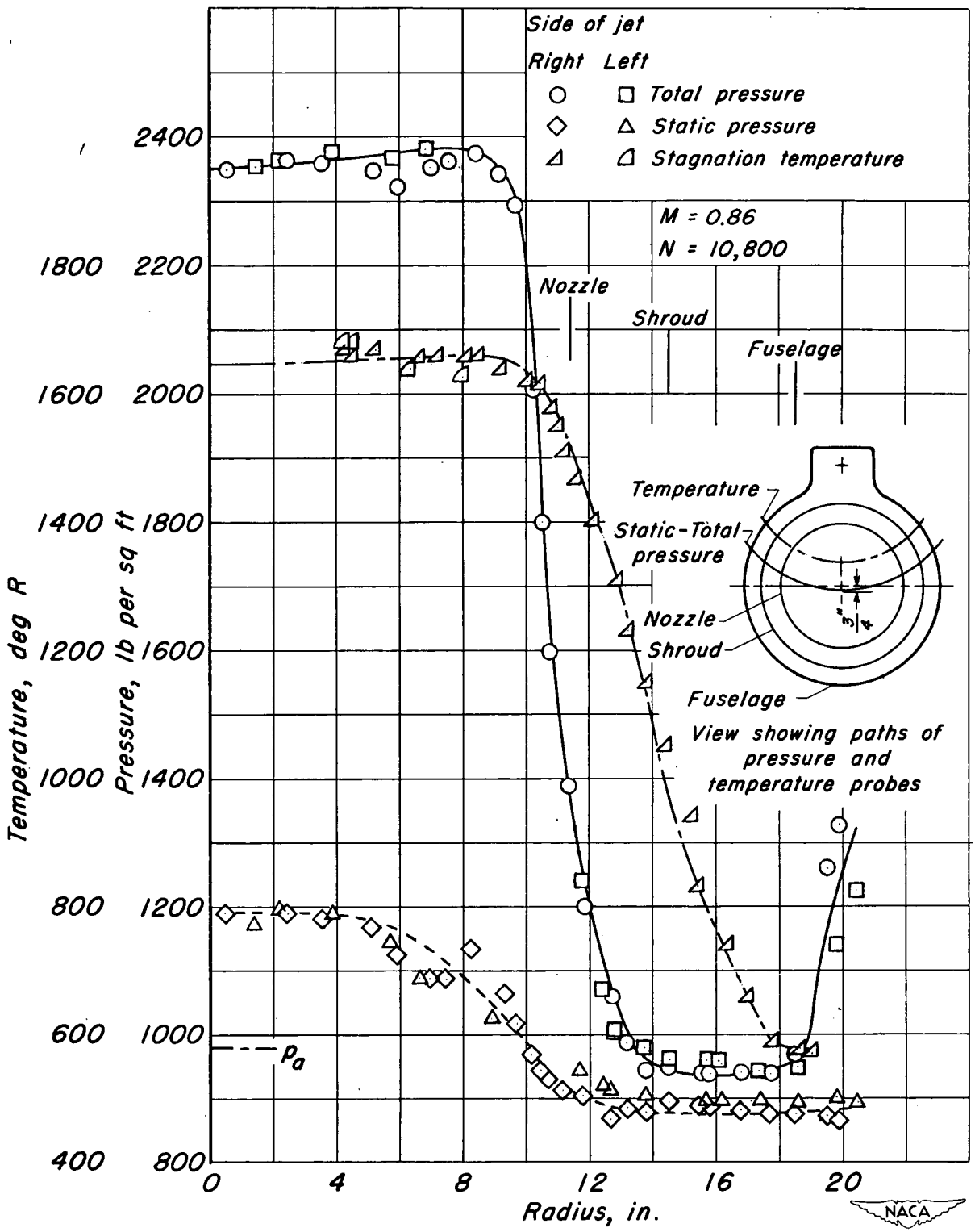

Figure 7.- Typical set of test data from Tail A, basic configuration, afterburner off.

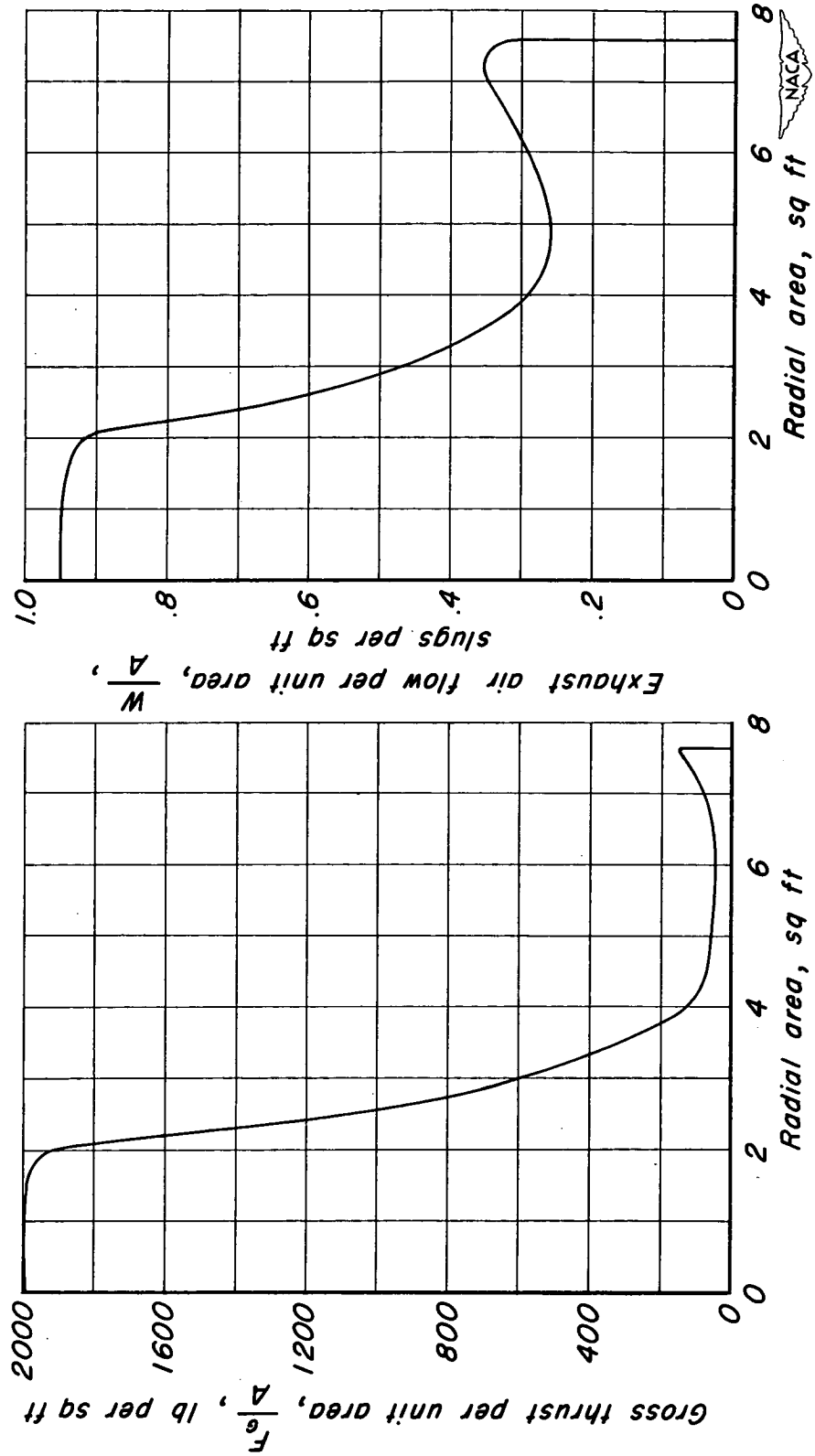

Figure 8.- Thrust and air-flow profiles for Tail A, basic configuration, afterburner off.

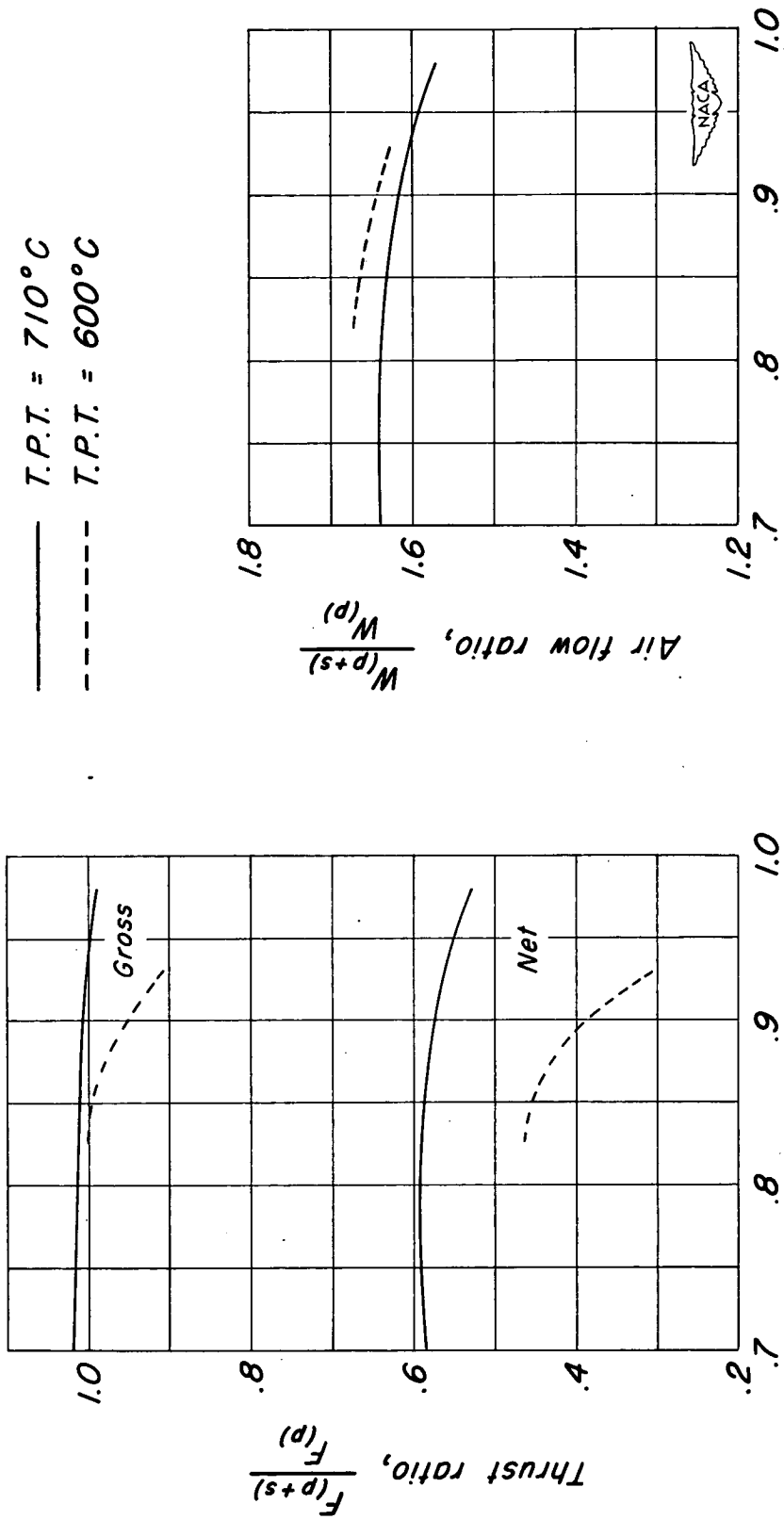

(a) Thrust characteristics.

(b) Air-flow characteristics.

Figure 9.- Ejector characteristics for Tail A, basic configuration, afterburner off.

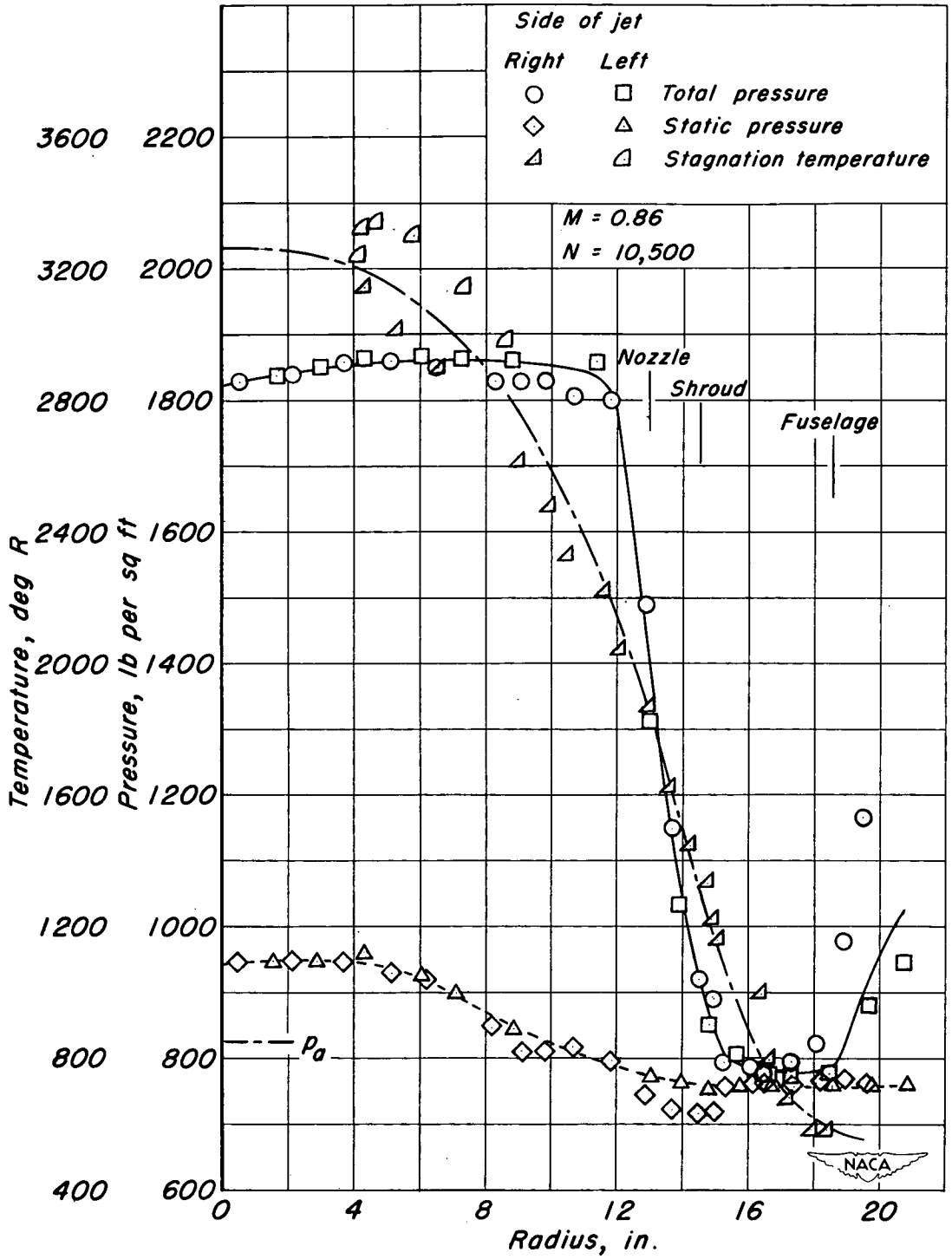

Figure 10.- Typical set of test data from Tail A, basic configuration, afterburner on.

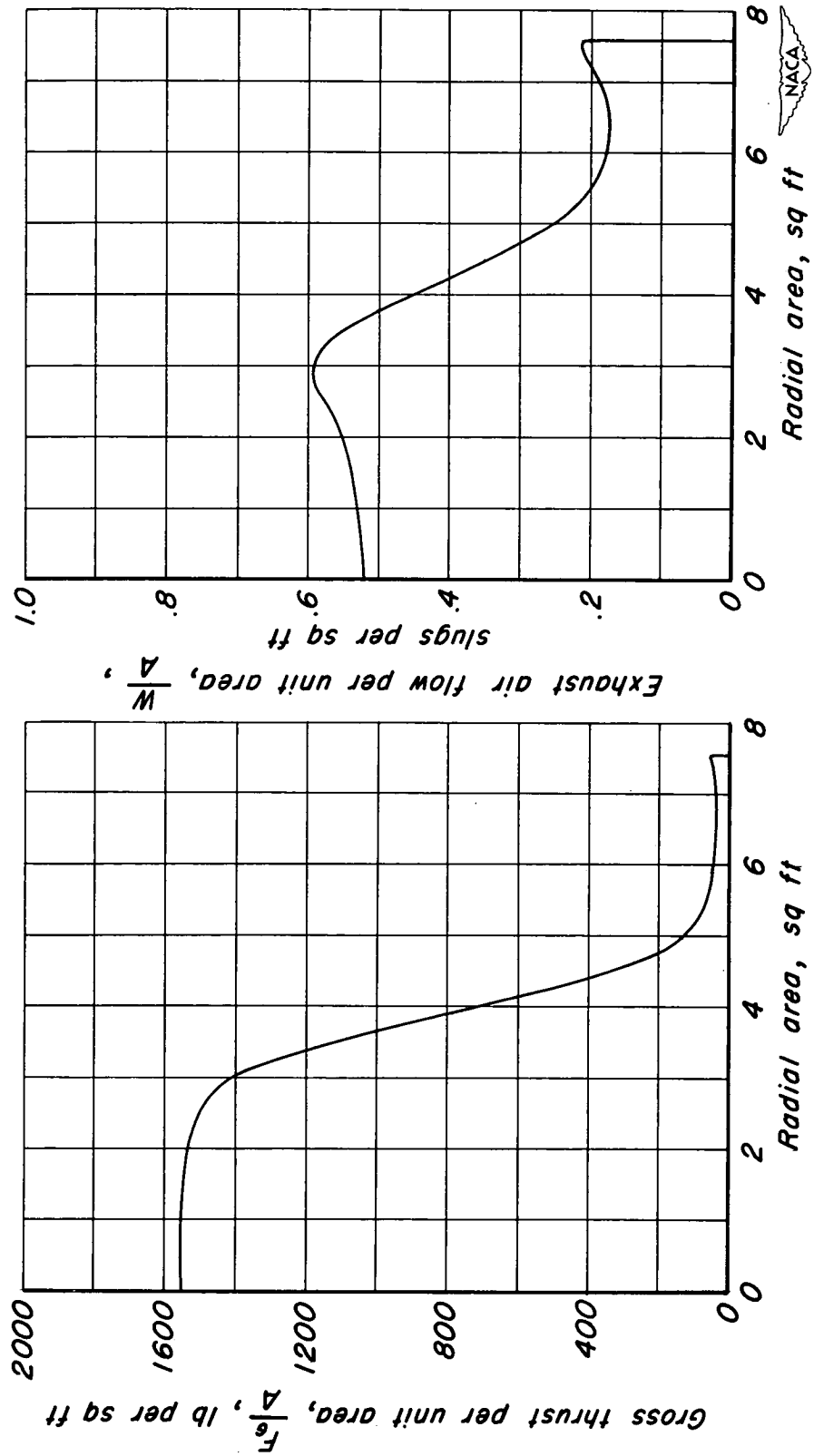

(a) Gross thrust.

(b) Air flow.

Figure 11.- Thrust and air-flow profiles for Tail A, basic configuration, afterburner on.

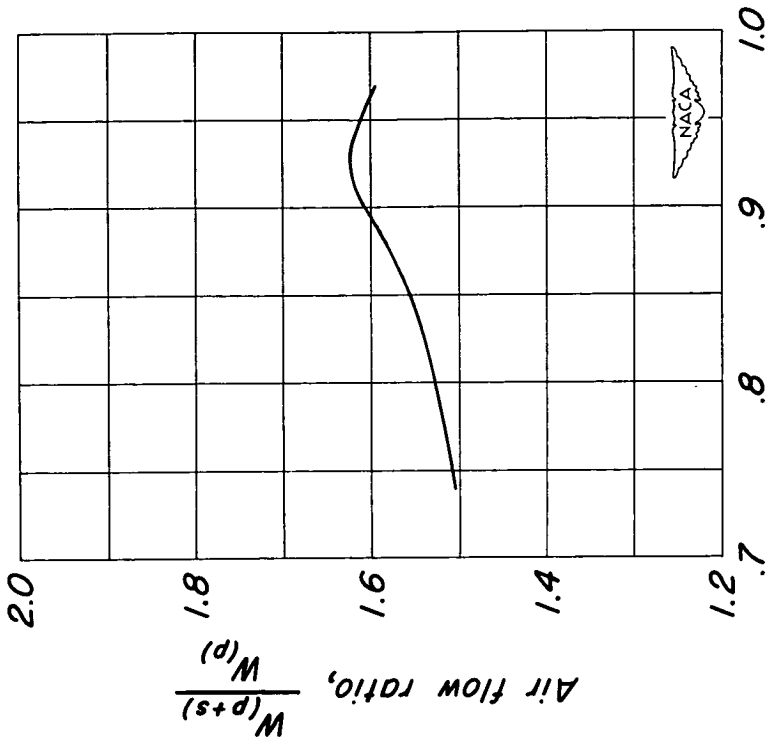

(b) Air-flow characteristics.

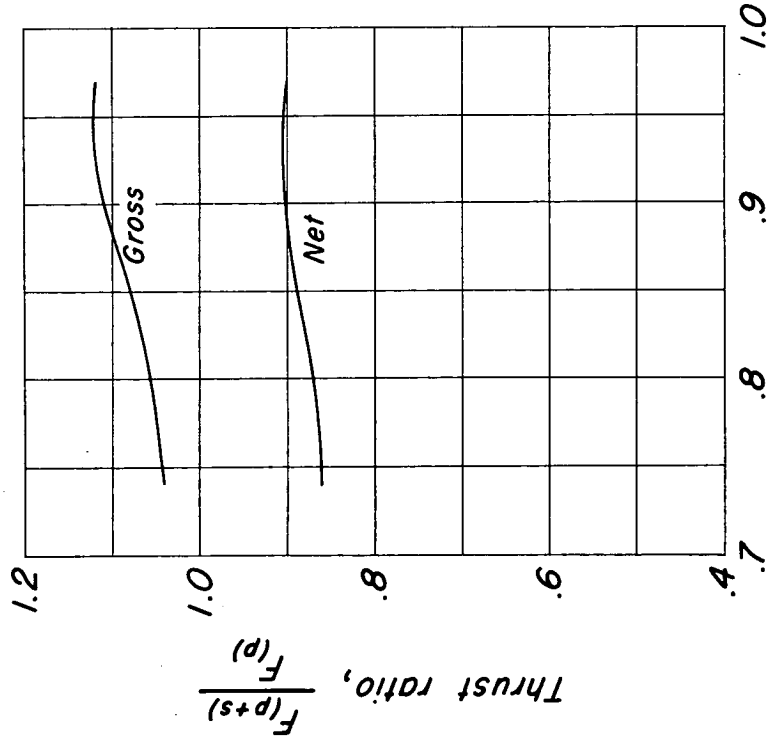

(a) Thrust characteristics.

Figure 12.- Ejector characteristics for Tail A, basic configuration, afterburner on.

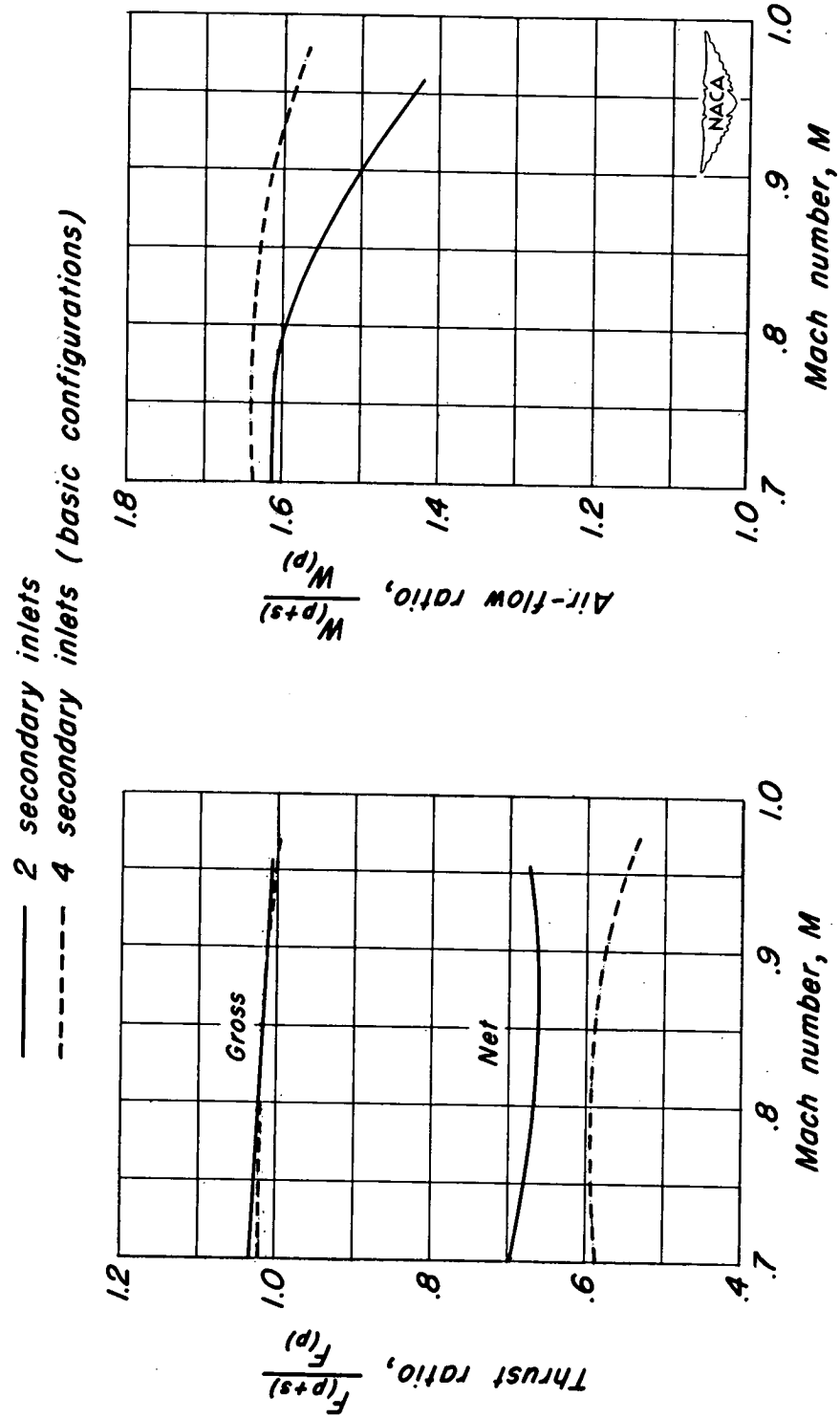

(a) Thrust characteristics.

(b) Air-flow characteristics.

Figure 13.- Effect of modifications on the ejector characteristics for Tail A, afterburner off. tail-pipe temperature 710° C.

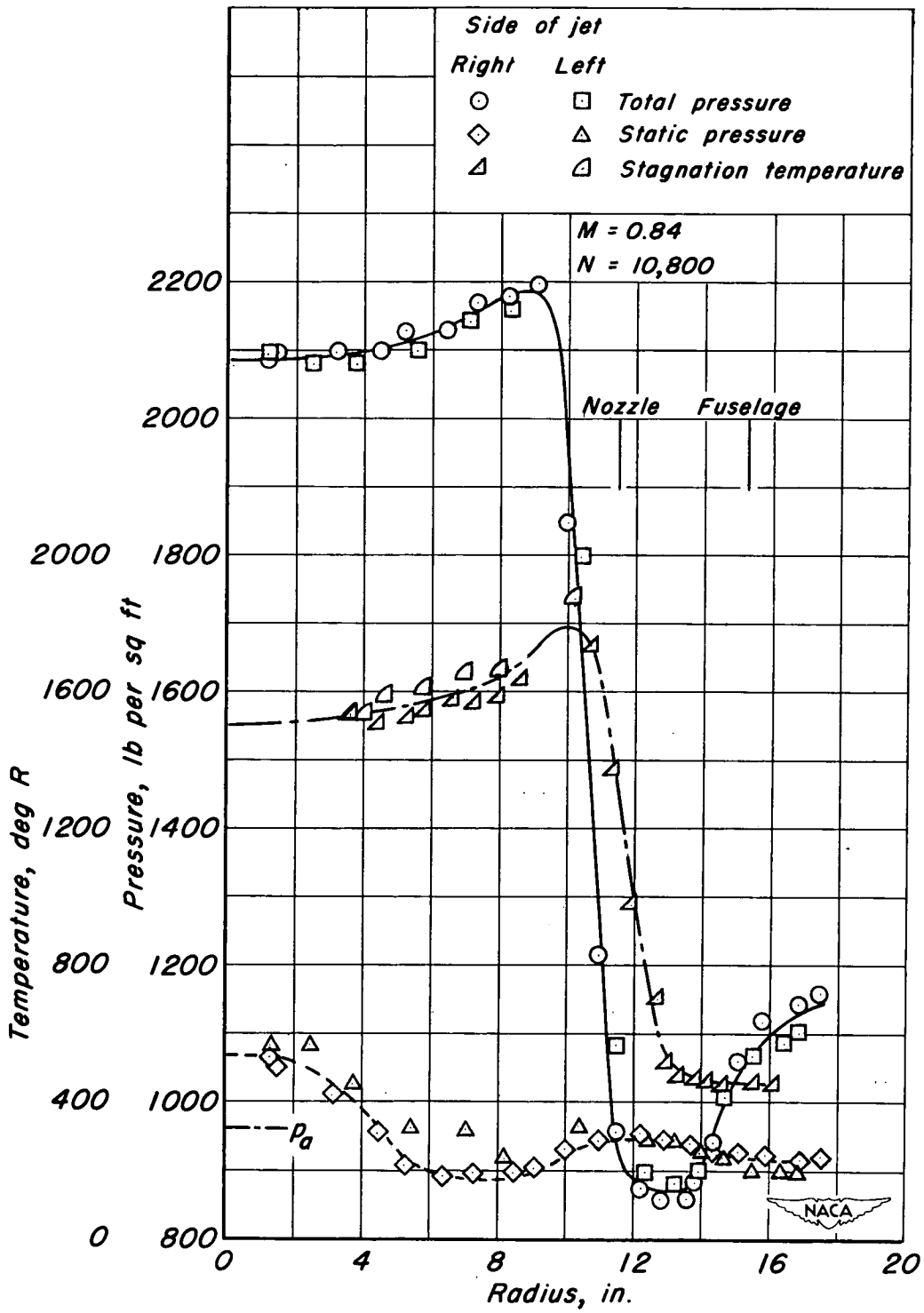

Figure 14.- Typical set of test data from Tail B, basic configuration, afterburner off.

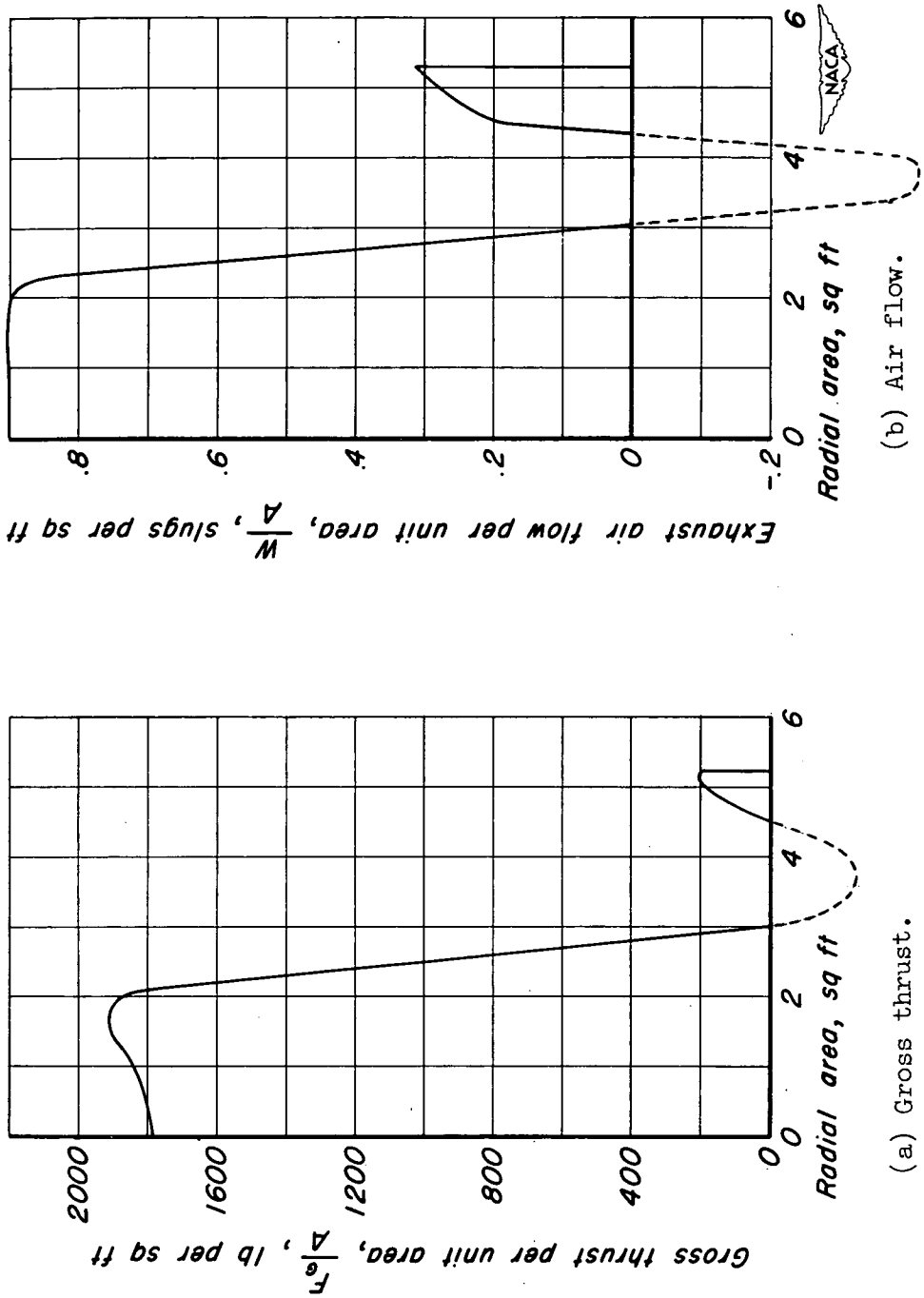

(b) Air flow.

(a) Gross thrust.

Figure 15.- Thrust and air-flow profiles for Tail B, basic configuration, afterburner off.

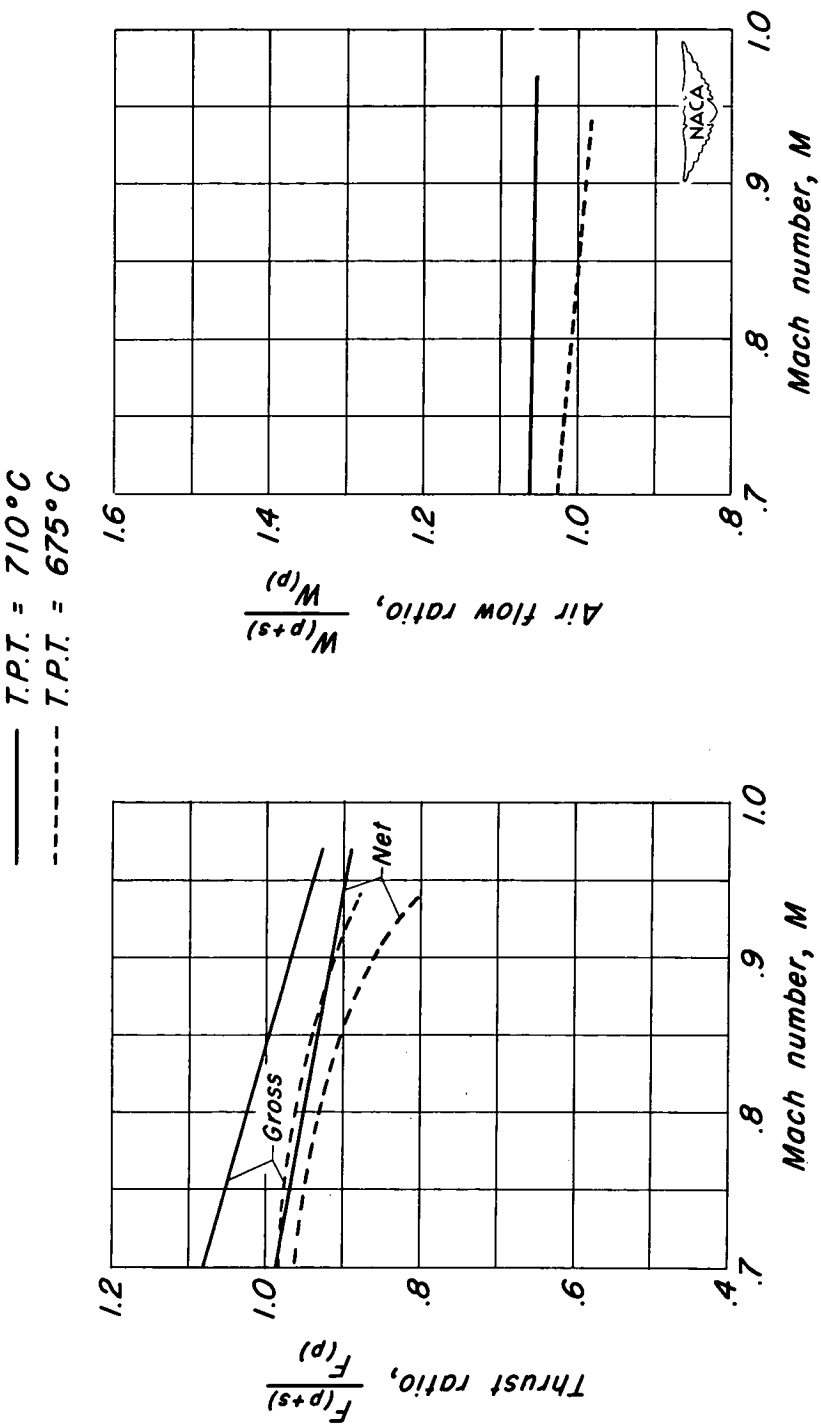

(a) Thrust characteristics. (b) Air-flow characteristics.

Figure 16.- Ejector characteristics for Tail B, basic configuration, afterburner off.

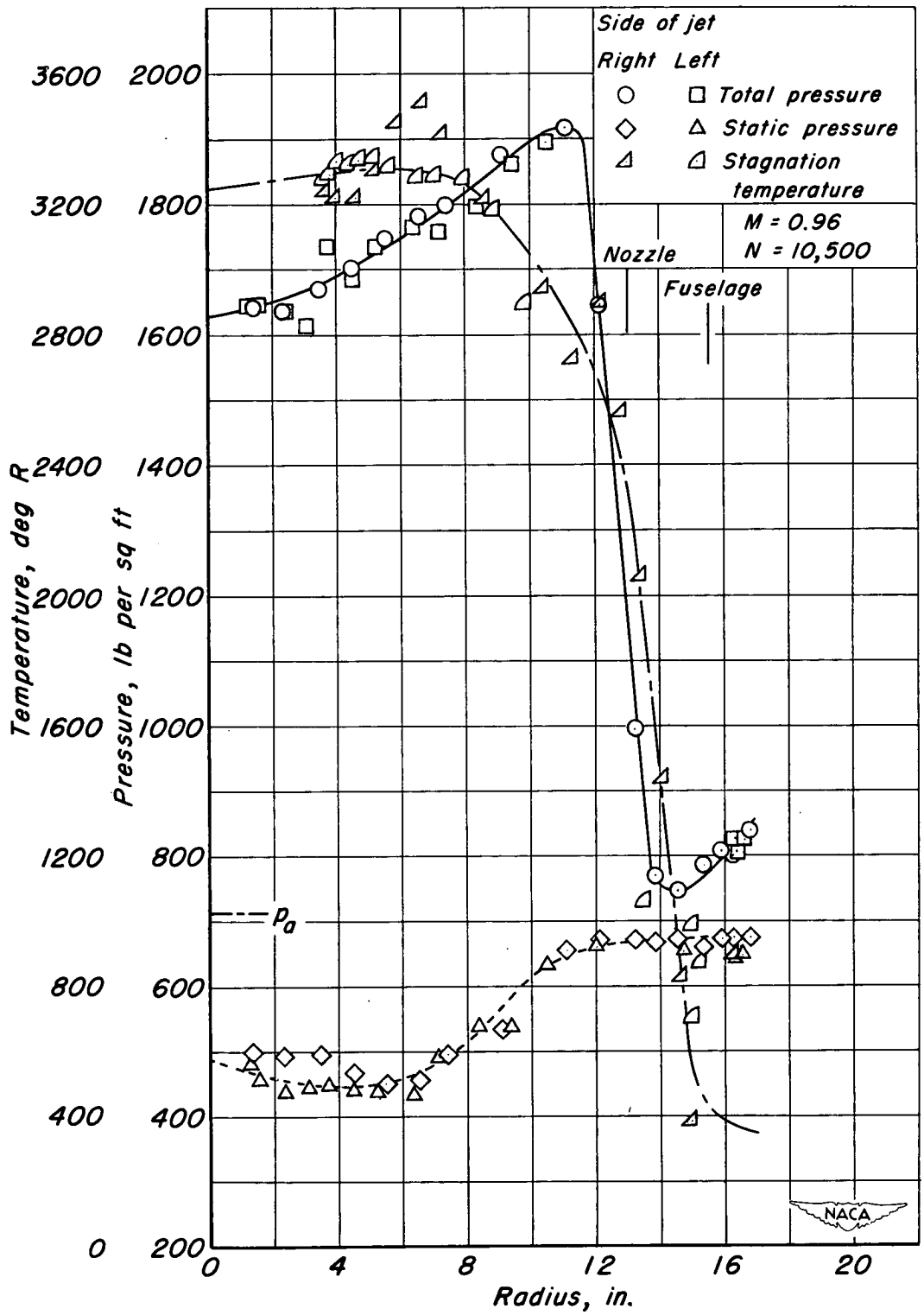

Figure 17.- Typical set of test data from Tail B, basic configuration, afterburner on.

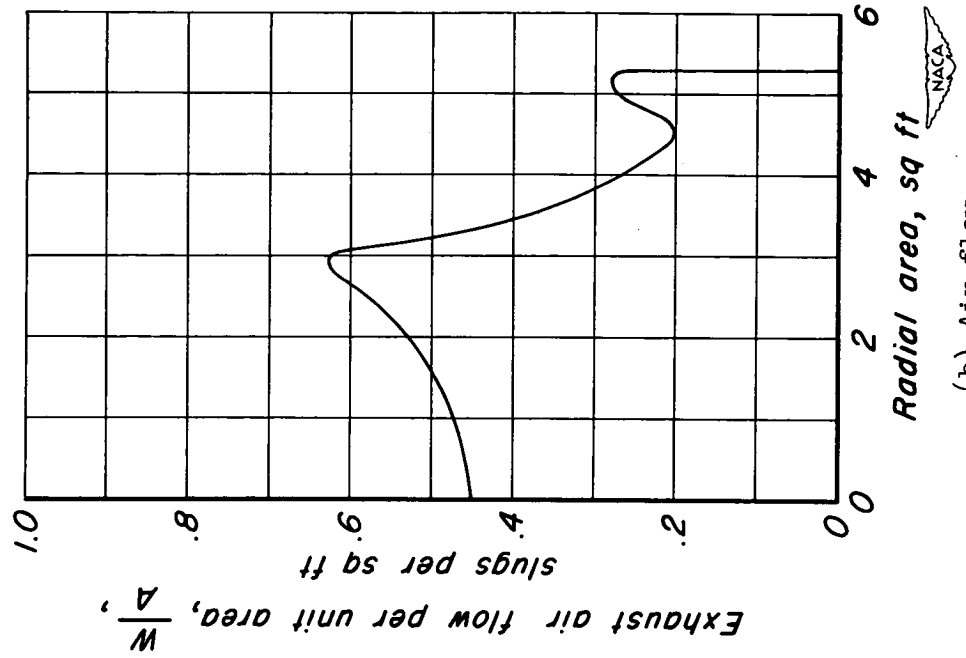

(b) Air flow.

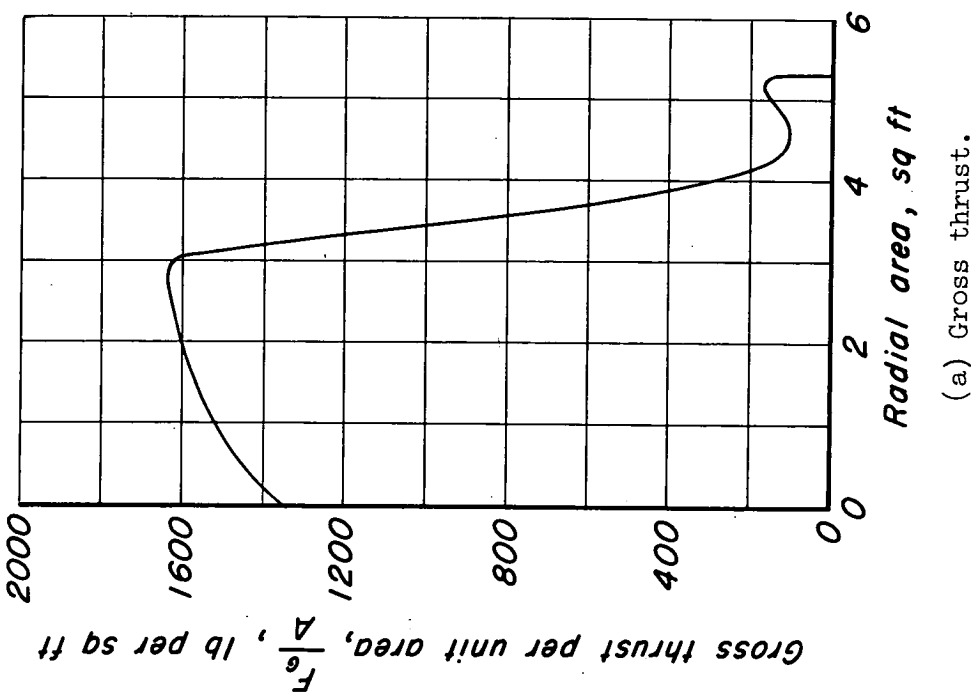

(a) Gross thrust.

Figure 18.- Thrust and air-flow profiles for Tail B, basic configuration, afterburner on.

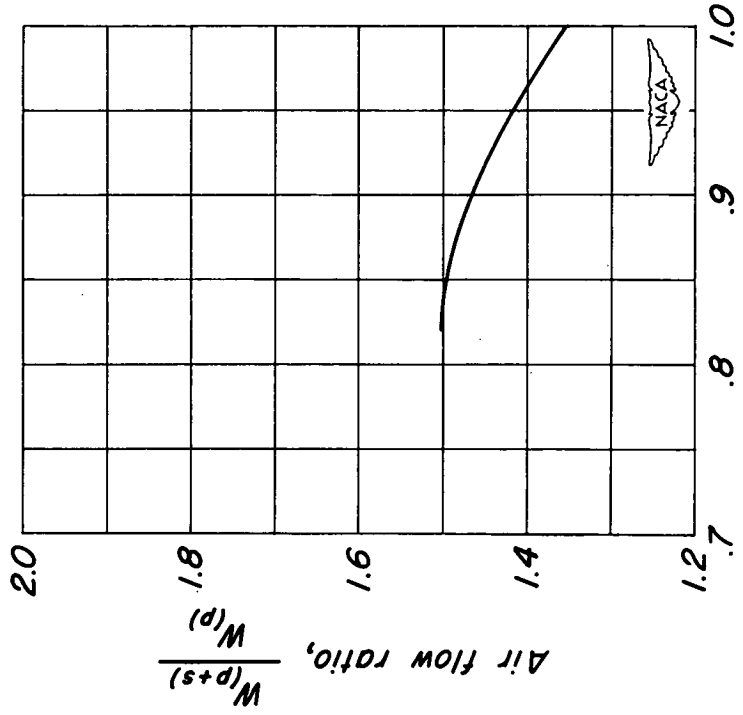

(b) Air-flow characteristics.

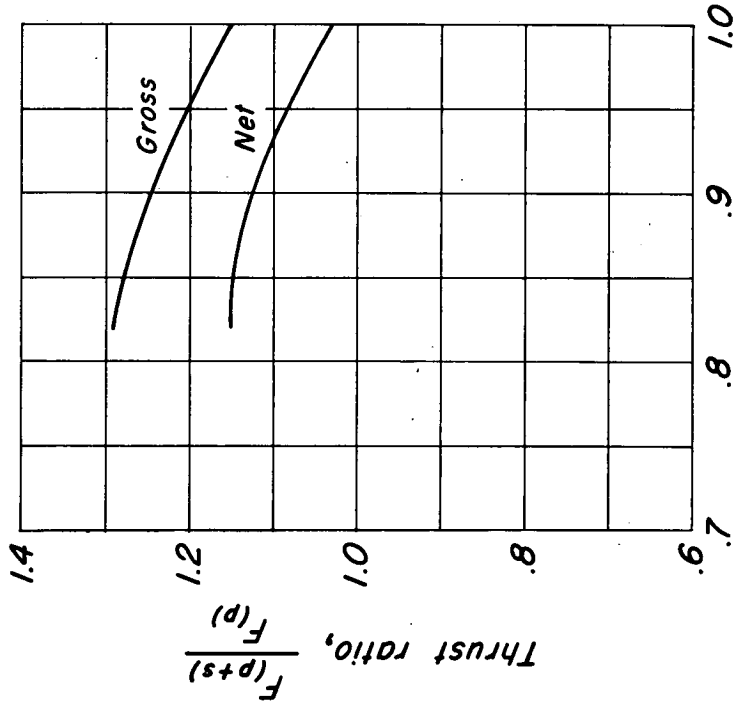

(a) Thrust characteristics.

Figure 19.- Ejector characteristics for Tail B, basic configuration, afterburner on.

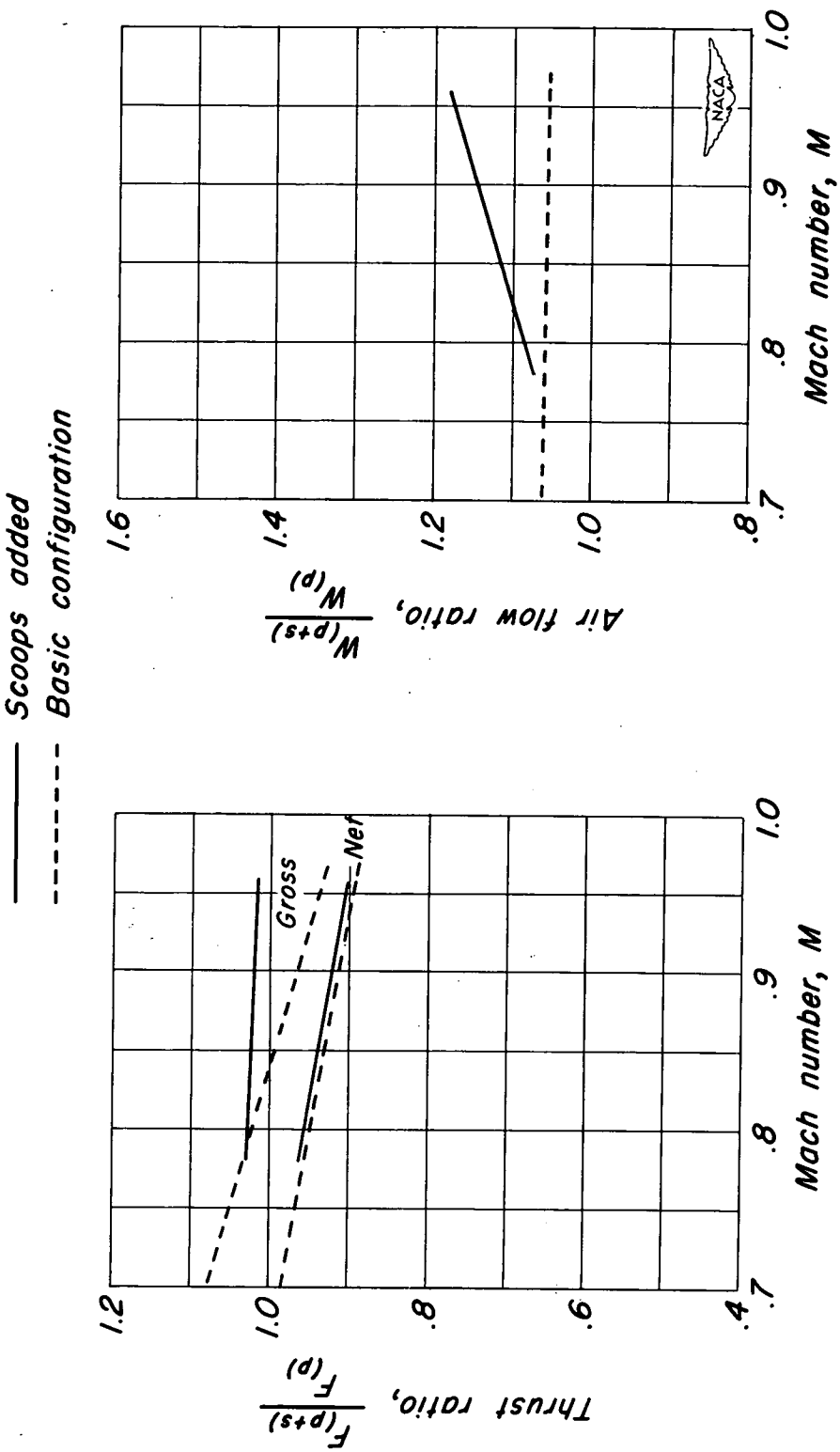

(a) Thrust characteristics.

(b) Air-flow characteristics.

Figure 20.- Effect of modifications on the ejector characteristics for Tail B, afterburner off, tail-pipe temperature 710° C.

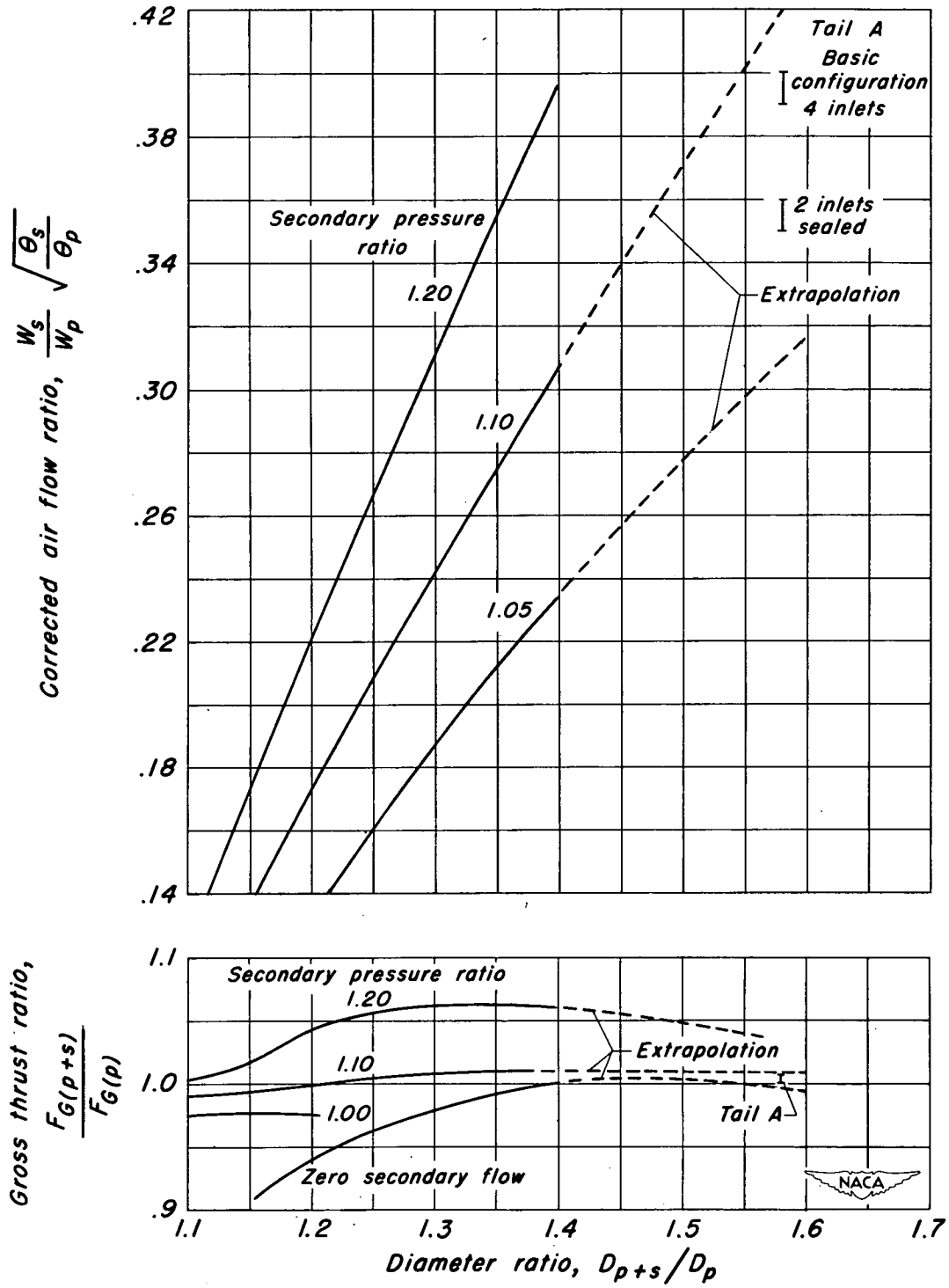

Figure 21.- Variation of air-flow ratio and gross thrust ratio with diameter ratio as determined on an ejector test stand; primary pressure ratio, 2.0; spacing ratio, 0.80.

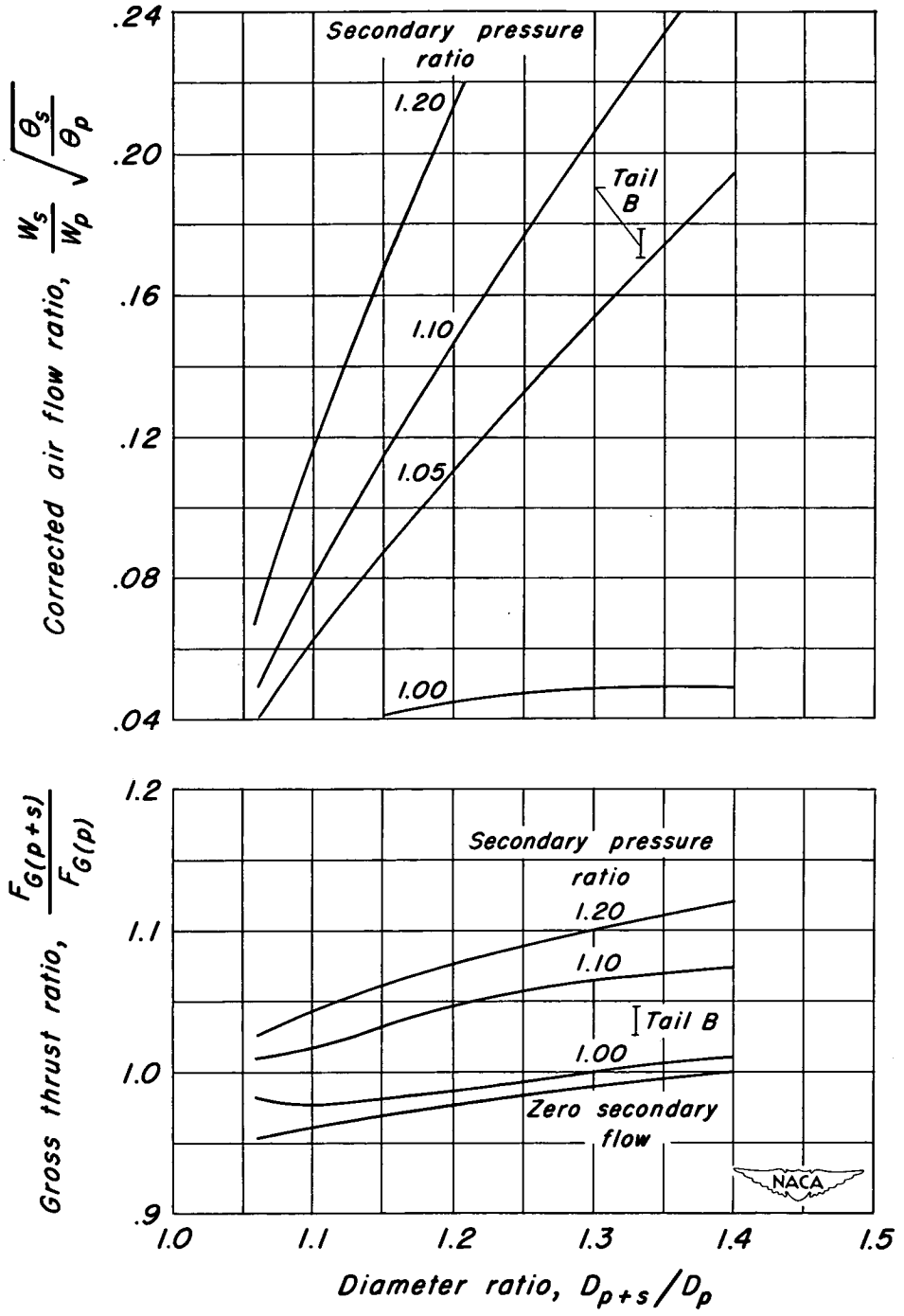

Figure 22.- Variation of air-flow ratio and gross thrust ratio with diameter ratio as determined on an ejector test stand; primary pressure ratio, 2.0; spacing ratio, 0.40.

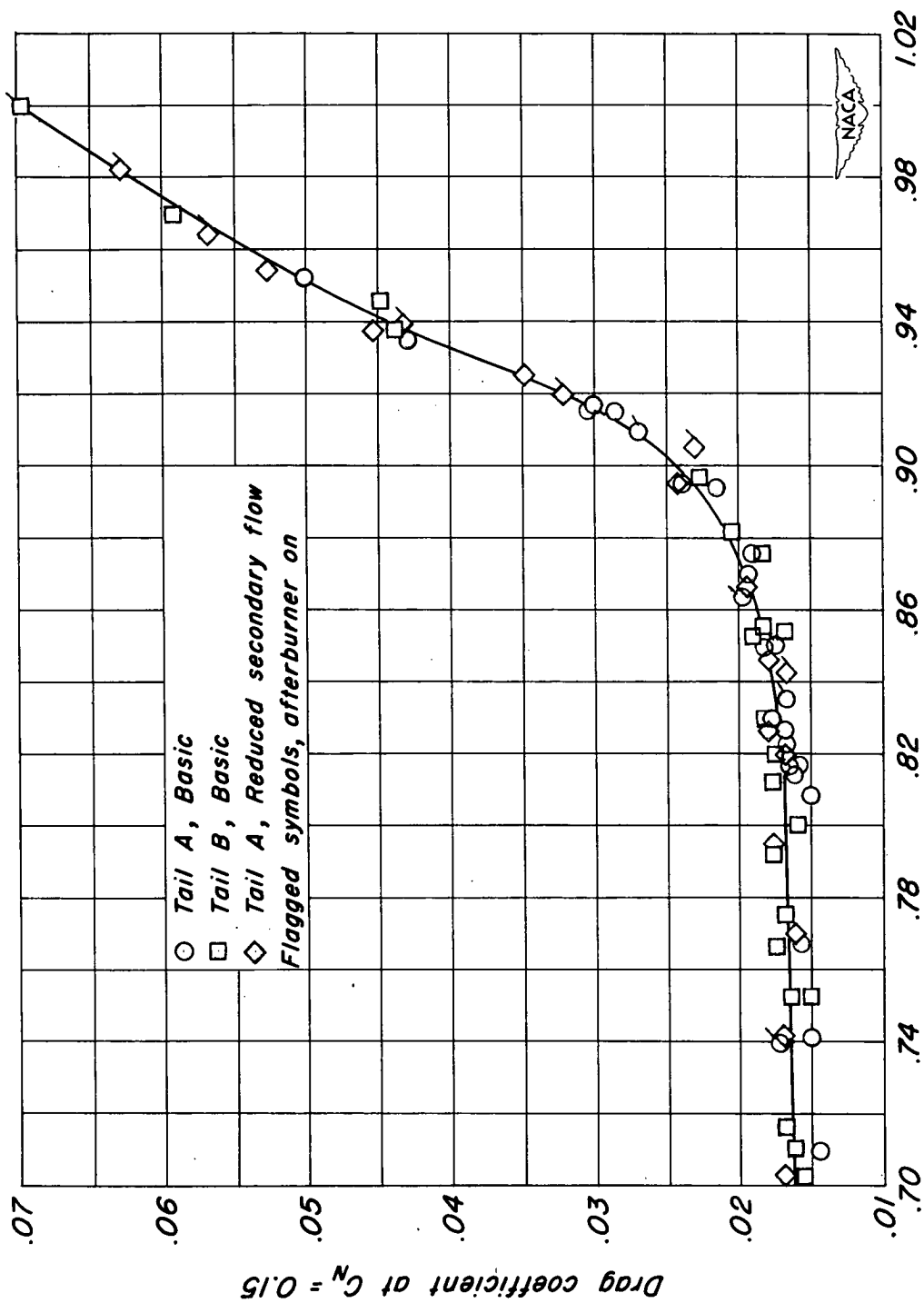

Figure 23.- Variation of airplane drag coefficient, as determined from ejector net thrust, with Mach number.

NACA-Langley - 3-15-54 - 325